GENETIC DETERMINANTS OF COXSACKIEVIRUS B3 PATHOGENESIS

April L Barnard

Submitted to the faculty of the University Graduate School
in partial fulfillment of the requirements
for the degree
Master of Science
in the Department of Microbiology and Immunology,
Indiana University

October 2020

Accepted by the Graduate Faculty of Indiana University, in partial fulfillment of the requirements for the degree of Master of Science.

Master's Thesis Committee

_____
Christopher M Robinson PhD, Chair

_____
Carmella Evans-Molina PhD., MD

_____
Andy Yu MD., PhD

© 2020

April L Barnard

DEDICATION

To all the inspiring women I call ‘doctor’ and to those who have earned the Ph.D. following their names. Specifically, this is dedicated to Elizabeth, Pamela, Gretchen, Emily, and Ruth all of whom I will never address so informally again; any failing belongs solely to me, but I tried my best because of you.

To Michael, you know what you did. Thank you for always encouraging me to swing for the fences. You have shown me that true parity in partnership can and does exist. Your continued support for all my endeavors, no matter how outlandish, gets me out of bed every morning.

To Agnes, who, quite honestly, made any success I may garner possible. Without you, Agnes, juggling motherhood and graduate school may have been impossible; I am so grateful for your love and steadfast support.

And finally, this work is dedicated to the singular reason I do anything in this life, my daughter Grace. My wish for you, banana, is that if you decide to enter a career in STEM, I hope you live in a world that will allow you to choose an all-female committee; may it not be an anomaly.

ACKNOWLEDGEMENT

The time that I have spent in the lab have helped me gain invaluable insight and perspective. I would like to use the next few paragraphs to thank the people who have supported me throughout the completion of my degree and those to whom I am grateful.

Firstly, I would like to thank the Indiana University Biomedical Gateway program for their support throughout my time in the graduate program. The sincerity with which the women in the graduate office conduct themselves is admirable and can be felt by all those they are there to aid. I would like to specifically thank Brandy Wood, Assistant Director, IBMG Program for PhD Study and Tara Hobson Director of Graduate Programs and Student Success. Without their guidance, patience, and discretion, I would never have lasted as long as I did. Brandy and Tara, I will miss the intimate Red Lion Grog House discussions during recruitment, you two were always a breath of fresh air.

To IUSM in general, thank you for always being accessible, whether it was 3 am or every weekend, your doors were always open to me. I would like to thank my supervisor Dr. Christopher Robinson who taught me that doors will always be closed to me, and that the trick is to find the door you really want to open. Thank you to my committee members Dr. Evans-Molina and Dr. Andy Yu; you have provided me with insightful expertise and for that I am grateful.

Finally, I would like to thank my parents, family, and friends for always asking me about my research and more importantly, pretending to listen to the response.

April L Barnard

GENETIC DETERMINANTS OF COXSACKIEVIRUS B3 PATHOGENESIS

Enteric viruses are among the most common infectious human viruses worldwide, causing an estimated 10-15 million infections per year in the United States. Among enteric viruses, Coxsackievirus is commonly isolated and can lead to the development of meningitis, encephalitis, pancreatitis, and hepatitis. Furthermore, Coxsackievirus B3 is the primary cause of viral myocarditis and can lead to pleurodynia, with nearly 40,000 symptomatic cases reported in the United States each year. The enteroviral ssRNA genome contains a 5' untranslated region (5'UTR) which consists of two structural components, the cloverleaf and the internal ribosome entry site (IRES), both shown to be integral to viral success. Additionally, the viral genome encodes four structural VP proteins as well as 11 non-structural proteins. Polymorphisms found within the CVB3 population have been linked to viral virulence. Here, we compare two CVB3 Nancy variants to elucidate the downstream effects observed in response to mutations found in the CVB3 genome. Implementing our novel oral inoculation model, we aimed to determine the impact mutations found in the 5'UTR and VP regions exert on viral pathogenesis. We also aimed to delineate the in vitro effects of the observed mutations. We investigated the role mutations found in the structural regions played in virus host cell attachment, in vitro cell viability, and replication. Our work has further confirmed the relevance and impact of mutations found in the VP region of the CVB3 genome.

Christopher M Robinson PhD, Chair

TABLE OF CONTENTS

LIST OF TABLES

LIST OF FIGURES

LIST OF ABBREVIATIONS

3' UTR	3' untranslated region
5' UTR	5' untranslated region
CAR	Coxsackievirus-adenovirus receptor
CVB3	Coxsackievirus B3
DAF or CD55	Decay accelerating factor
DCM	Dilated Cardiomyopathy
eIF	eukaryotic Initiaion Factor
EV	Enterovirus
GI	Gastrointestinal
IP	Intraperitoneal injection
IRES	Internal Ribosome Entry Site
mRNA	messenger RNA
PDB	protein databank
PV	Poliovirus
RD	Rhabdomyosarcoma

RV	Rhinovirus
ssRNA	single stranded RNA
TNF-a	Tumor necrosis factor alpha
VPg	viral protein, genome linked
WT	Wild type

CHAPTER ONE

1. Introduction

1.1 Picornavirus Background

Enteric viruses or those human viruses primarily transmitted via fecal–oral route either from person-to-person contact or by ingestion of contaminated food or water, continue to be a significant cause of morbidity and mortality worldwide [1, 2]. Enteroviruses, a prevalent subset of enteric viruses, belong to the *Picornaviridae* family. The *Picornaviridae* family comprises a group of small single stranded RNA viruses such as poliovirus (PV), coxsackievirus (CV), and enterovirus-71 (EV-71) that display a wide variety of tissue tropism and cause significant disease. Also within the *Picornaviridae* family is human rhinovirus, the causative agent of the common cold, a relatively mild disease that nevertheless costs the US economy nearly $40 billion each year [3]. In additional to financial burden, some *Picornaviridae* family members are capable of inflicting deadly disease, such as the seasonal epidemics of enterovirus 71 that affect Asian and Pacific regions.

Whereas global efforts to eradicate poliovirus have proven successful, still other dangerous and costly picornaviruses continue to circulate widely. For example, in recent years massive outbreaks of Enterovirus D68 (EV-D68) have become common in the US, Europe and Asia and human parechovirus 3 (PeV-A3) outbreaks have been observed in Australia [4-6]. Importantly, Enterovirus A71 (EV-A71) outbreaks have occurred in Asia and resulted in high illness and death rates among children [7]. These outbreaks of various picornaviruses are associated with severe disease and demonstrate the real threat non-polio picornaviruses continue to pose to human health [8]

Human picornaviruses are primarily transmitted via the fecal-oral route or via respiratory transmission. Initial viral infection is thought to originate in the respiratory tract and/or the gastro-intestinal tract, followed by spreading via the blood to infect various target organs such as skin, heart, or brain [9]. Apart from rhinoviruses (RVs), human picornaviruses display broad tissue tropism. Whereas significant progress has been made in identifying several cellular receptors [10-12], many of the mechanisms regarding viral entry events remain largely unknown.

The positive sense single stranded RNA genome of picornaviruses is a relatively small 7.5 to 10 kb [13] resulting in just four structural proteins and seven non-structural proteins [10, 14, 15]. In 1985, thanks to innovations in x-ray crystallography, Rossman, M., et al. solved the atomic resolution structure of human rhinovirus 14, making the picornavirus genome the first animal virus 3D structure to be illuminated [16, 17]. Among the discovered novel viral structures in the picornavirus genome were predicted locations for receptor binding as well as several antigenic sites [14, 17]. Subsequent research focused on solving the structures of other viruses belonging to the *Picornaviridae* family revealed highly conserved areas of the genome, thereby allowing the assumption that the antigenic sites established for rhinovirus would also be found in other picornaviruses such as Coxsackievirus [14, 18-20]. Due to their high level of adept adaptability, promiscuous nature of transmission, and overall prevalence, however, picornaviruses have proven difficult to treat and eradicate. Still, the conservation of certain viral proteins provides hope for broad-spectrum antivirals [10, 21, 22]. Though there have been numerous attempts to develop compounds designed to target different points in the viral lifecycle, currently, no such antivirals exist [10, 21, 22].

1.2 Coxsackievirus History and Significance

Coxsackievirus gets its name from the Hudson river town of Coxsackie, New York, where in 1947, a suspected polio epidemic turned out to have a different viral genesis. After isolating virus from fecal specimens of two young boys suffering flaccid paralysis, Gilbert Dalldorf and Grace Sickles reported a novel virus capable of causing polio-like flaccid paralysis [23, 24]. Over the next year, Coxsackievirus A (CVA) was identified as producing a generalized and widespread myositis mainly affecting the striated muscles. Subsequently, Edward Curnen, Ernest Shaw and Joseph Melnick discovered yet another antigenically dissimilar novel virus and termed this virus Coxsackievirus B (CVB) [25]. Whereas CVA was thought to mainly affect striated muscle, CVB not only induced a focal and limited myositis in striated muscles, but also produced degeneration of brain, pancreas, heart, muscle and embryonic fat pads under the skin in baby mice [24-26]. Between its discovery in 1947 and today, 23 CVA and six CVB serotypes have been identified. Among the CVB3 Nancy strain, several strain variants have been characterized based on polymorphisms found within the CVB3 population (Table 1).

Assession #	CVB3-Nancy Strain	Description	Receptor Preference	Citation
AF231764	**P**	Parental strain isolate capable of establishing a persistent carrier-state infection without visible cytopathic effect in HuFi H	CAR	Schmidtke et al., 2000
AF231765	**PD**	derivative of CVB3/P	DAF	Schmidtke et al., 2000
AF231763	**31-1-93**	derivative of the CVB3/PD strain	CAR/DAF	Merkle et al., 1999
M88483	**20 Klump/Tracy**	cardiovirulent	CAR	Lindberg et al., 1986
AY752945	**0**	avirulent; derivative of CVB3/20	CAR	Gauntt et al., 1979
AY673831	**GA**	infectious cDNA-generated; avirulent	CAR	Lee et al., 2005
AY752944	**28/HA**	hemagglutinating CVB3 variant	DAF	Goldfield et al., 1957
JN048469	**RD**	infects and lyses RD cells	DAF	Lindberg et al. 1992
KJ025083	**MKP**	cardiovirulent	CAR	Liu et al., 2014
KC481610	**AH30**	isolated from patient with encephalitis complications following HFMD infection	CAR	Zhang et al., 2013
U57056	**H3**	cDNA-generated; highly myocarditic Woodruff variant	CAR	Knowlton et al., 1996

Table 1: CVB3 Nancy strain variants. Characterization of 11 fully sequenced CVB3 Nancy strain variants. Receptor preference indicates viral ability to use CAR and/or DAF to enter host cell.

1.3 Coxsackievirus Prevalence

Among the most ubiquitous enteric viruses isolated, Coxsackievirus (CV) is capable of inflicting significant disease, especially in young children and infants [1, 27, 28]. In fact, CV is the most frequently isolated virus among the estimated 10-15 million enteric viral infections per year in the United States [2] [27]. Due to the fecal-oral nature of transmission, most humans are infected with CV by the age of 5 suffering only mild, flu-like symptoms. Although the majority of CV infections are self-limiting and resolve without issue, CV is capable of infecting a range of tissues including the heart, pancreas and central nervous system [15] implicating it in a vast swath of diseases such as hemorrhagic conjunctivitis, hand, foot, and mouth disease, as well as viral myocarditis [29-31]. Research suggests CVs may play a role in severe systemic inflammatory diseases such meningoencephalitis, pancreatitis, and myocarditis [15, 32]. Additionally,

the consequences of CV infection during pregnancy can range from fetal myocarditis to neurodevelopmental delays in the newborn infant [33, 34]. Importantly, infants infected with CV have been shown to be extremely susceptible to myocarditis, meningitis and encephalitis with a subsequent mortality rate as high as 10% [35]. Coxsackievirus B3 (CVB3) is the most commonly isolated virus implicated in inflammation of the myocardium, known as viral myocarditis [29-31]. Viral myocarditis can develop into dilated cardiomyopathy and ultimately may result in the need for a heart transplant.

1.4 Coxsackievirus Structure and Lifecycle

Coxsackieviruses belong to the Enterovirus genus within the *Picornaviridae* family. Known enteroviruses that tend to infect internal organs comprise three polioviruses, 23 Coxsackieviruses group A, and six Coxsackieviruses group B. Among the six serotypes of CVB, only three, CVB1, 3 and 5, are notably cardiotropic or able to infect heart tissue [24, 36]. The roughly 30 nm in diameter icosahedral capsid of CV is composed of four structural proteins VP1, VP2, VP3 and VP4. The outer layer of the capsid is comprised of VP1, VP2 and VP3, whereas VP4 is an internal protein. Inside the capsid, the positive sense single stranded RNA ((+)ssRNA) viral genome is approximately 7.5 kb. The ssRNA is naturally infectious due to its positive-sense, resembling host messenger RNA (mRNA). The ssRNA comprises an open reading frame (ORF), flanked on both sides by 3′ and 5′ termini untranslated regions (UTRs). Importantly, the ORF contains genes encoding 11 proteins, four structural VP proteins and seven various non-structural proteins [37, 38]. In addition to the four structural capsid proteins, the genome encodes for two viral proteases (2A, and 3C), an RNA-dependent-RNA-polymerase (3D), two proteins involved in RNA synthesis (2B and 2C),

a primer for initiation of RNA synthesis (3AB) and a small polypeptide VPg (viral protein linked to the genome) (Figure 1). The covalently bound VPg found in the 5' UTR is essential to viral translation and replaces the 7-methylguanosine triphosphate cap structure employed by eukaryotic mRNA to initiate protein translation at the ribosome [24, 38, 39].

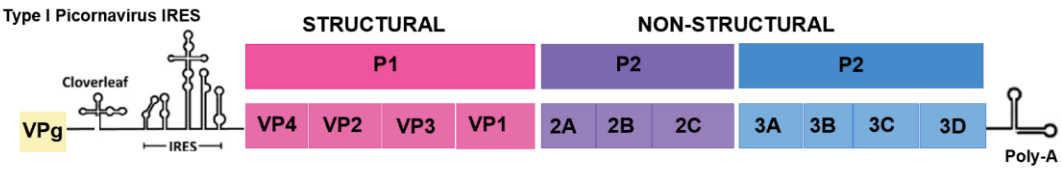

Figure 1: Schematic representation depicting the Enterovirus genome. There are two untranslated regions that flank a single large polyprotein coding region. The polyprotein product is divided into three sections: P1, P2, and P3. The P1 region contains capsid proteins while the P2 and P3 regions contain the nonstructural proteins and VPg (protein 3B). Following enzymatic cleavage, the polyprotein renders eleven mature final protein products.

CV entry into host cells is most commonly dependent on virus interaction with the host-cell receptors Coxsackievirus-adenovirus receptor (CAR), and in many polarized cell types, interactions with co-receptor decay-accelerating factor (DAF) [40, 41]. Other receptors, such as heparan sulfate, may also play a role in viral attachment to the host cells [24, 42]. Situated within the tight junctions between polarized intestinal epithelial cells, CVs main receptor, CAR, is largely inaccessible to the virus. To reach CAR in the gut CV will bind to DAF, triggering a series of events that lead to viral entry. Briefly, upon binding, DAF initiates Ab1 kinase activation resulting in the clustering of DAF molecules and the induction of actin rearrangement. Actin rearrangement in the host cell facilitates the movement of CV between host cells and into the tight junctions where is can interact with CAR [10, 24]. Upon entry into host cells, endosomal pH changes induce viral uncoating, liberating the (+)ssRNA viral genome to be translated and transcribed.

Initially, the CV genome is translated as a large polypeptide that is eventually cleaved into the individual structural and nonstructural proteins in the cytoplasm by the virus-encoded proteases 2A, 3C, and 3CD [10, 43, 44]. Genome replication by the RNA-dependent RNA polymerase 3D polymerase starts with the synthesis of a (-) strand copy of the incoming viral genome to generate a double-stranded RNA replication intermediate. The new strand thereby serves as a template for the production of new (+) strands, which will continue to serve as a template for further translation and replication or be encapsulated into new virions (Figure 2). The structural capsid proteins, VP0, VP1 and VP3 assemble into protomers and pentamers and together with the (+)ssRNA form the provirion. Finally, RNA induced processing of the VP0 protein into VP2 and VP4 yield mature virions completing the life cycle and release of viral progeny for further infection of neighboring cells [24].

Once inside the host cells, CV rapidly shuts down cellular RNA and protein synthesis. Moreover, previous studies have revealed that the 5′ and 3′ UTRs play a major role in regulation of viral RNA synthesis. The unusually long 5′ UTR contains several stem-loop structures, particularly the highly conserved stem-loop I, that play a critical role in enterovirus genomic RNA synthesis [45, 46]. Deletion mutations made to these stem-loop regions in CVB3 RNA allowed viral translation, but not RNA synthesis [47]. Finally, several laboratories have confirmed a role for the ERK1/2 pathway, whose phosphorylation is required for CVB3 infection [48-50]. A member of the mitogen-activated protein kinases (MAPKs), ERK1/2 plays an important role in regulating biological events such as cell proliferation, differentiation and stress responses [51].

Importantly, studies have revealed that the early activation of ERK1/2 may result from the engagement of CVB3 with its main receptor CAR, co-receptor DAF or both [48, 50].

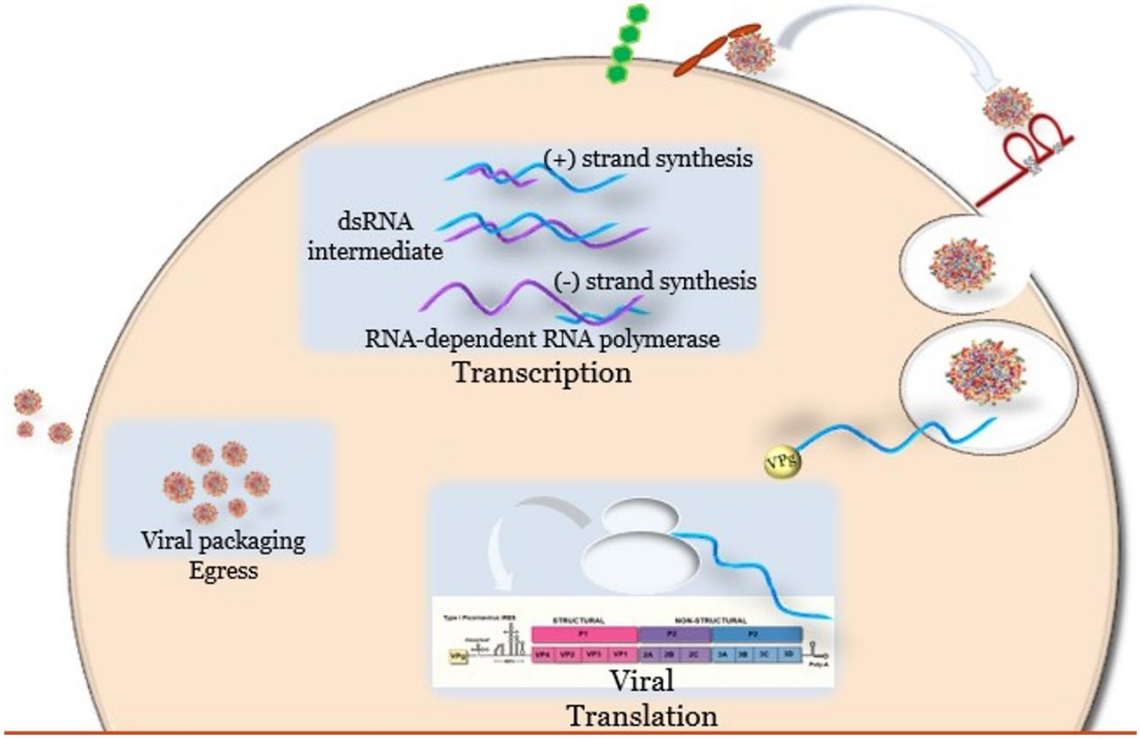

Figure 2: Schematic representation depicting the Coxsackievirus lifecycle. Cell entry: Interaction with its main receptor, CAR, triggers CV endocytosis into the host cell. In the case of polarized gut epithelial cells, CV may interact with the co-receptor DAF and be shuttled to CAR which is located between tight junctions. Synthesis: The CV (+)ssRNA is liberated from the capsid in the host cell cytoplasm where it will begin transcription and translation. Egress: The viral capsid is assembled and CV (+)ssRNA is packaged within the capsid and viral progeny is released for further infection of neighboring cells.

1.5 Further Research

Despite progress, critical characteristics of the enterovirus infection within the human gastrointestinal system remain obscure. Importantly, both viral and host factors affecting incidence, severity and pathogenic mechanisms of CV infection remain elusive [52]. Although elucidation of host factors influencing the disease process has progressed, there are still many remaining unanswered questions regarding the influence of viral genetics on host cell entry, viral replication, viral translation, and pathogenesis. In

addition, a structure-based mechanism describing how these interactions mediate virus multiplication and virulence remains unknown [53]. Finally, the molecular mechanisms involved in the tissue tropism of CVs as well as their ability to persist in the host remain unclear despite the potential unknown lasting consequences of CV infection [15].

Due to the inability to proofread and edit genomic errors incurred during viral replication, the CV genome suffers a relatively high error rate (10^{-4} substitutions per nucleotide per cell infection (s/n/c)). CV phenotypes that arise as a result of mutations are categorized by the ability of a particular strain of virus, experimentally propagated in various cell lines, to rapidly diverge and develop preference for either one or both CV receptors [8, 49]. Continued research regarding mutations found within the CV genome and the role of these genetic determinants play in CV pathogenesis is still urgently required.

CHAPTER TWO

2. Polymorphisms within the Coxsackievirus B3 population

2.1 Picornavirus mutations

A relatively stable non-enveloped virus, CVB3 is transmitted via the fecal-oral route and can withstand the acidic environment of the stomach. A general lack of knowledge regarding the genesis of infection, however, makes it difficult to accurately map the precise viral pathogenesis. Nonetheless, previous research suggest CVB3 infection originates in the GI and proceeds to periphery organ systems via viremia. Similar to other enteroviruses, the CVB3 genome can be organized into the following four major regions: a 742 nucleotide 5' untranslated region (5' UTR), a single open reading frame encoding a 2185 amino acid polypeptide, a 98 nucleotide 3' UTR with a highly polyadenylated end region (polyA tail) [54, 55]. Additionally, virulence determinants have been identified in the enterovirus genome regions encoding structural and non-structural proteins including within the capsid proteins VP1–VP4 coding as well as in the non-structural protein coding regions [53, 56] (Figure 1).

To understand the impact of CVB3 infection, research has primarily focused on the study of viral genomics, virulence factors and their direct injurious effects on host tissue architecture, organ function, and immune response [49]. Due to their small size, many microbial genomes, including those of CVs have previously been sequenced [57], directing CVB3 research toward "post-genomic" phases of investigation for the previous two decades [49]. Despite the expansive tenure of research, many questions regarding CVB3 pathogenesis remain unanswered. Therefore, the study of CV mutations and their

downstream effects prove invaluable in the elucidation of mechanisms impacting CVB3 infection, the production of novel therapies, as well as potential vaccines.

2.2 Genetic mutations found in the 5' UTR region of the Enterovirus genome

As with most enteroviruses, the 5'UTR of CVB3 forms a highly ordered secondary structure that plays an integral role in controlling viral transcription and translation. Due to its critical role in all stages of the viral infection cycle, the structure and role of the picornavirus 5' UTR has been extensively studied. The EV 5' UTR is divided into seven domains that are further subdivided into two functionally distinct regions. The CVB3 RNA genome, like other EV's, contains an internal ribosome entry site (IRES) in the 5′ UTR region. Crucial to CVB3 translation initiation, IRESs are RNA elements that mediate end-independent ribosomal recruitment to internal locations within mRNA (Figure 3). Structurally related viral IRESs use distinct mechanisms based on non-canonical interactions with eukaryotic initiation factors (eIFs) and/or the eukaryotic 40S ribosomal subunit. Enhanced by eIF4A, IRES types 1 and 2 initiate translation via specific binding to the central p50 domain of eIF4G. The eIF4G–eIF4A complex recruits 43S complexes to the type 1 and type 2 IRES absent involvement from eIF4E. The type 3 IRES initiation, on the other hand, involves interaction with eIF3 and 40S subunit components of 43S ribosomal complexes. Consequently, the type 3 IRES directly attaches 43S complexes to the initiation codon independent of eIF4F, eIF4B, eIF1 and eIF1A.

Finally, because the 40S subunit's P-site is occupied by an IRES domain that mimics codon-anticodon base-pairing, the type 4 IRES can bind directly to 40S subunits thereby facilitating initiation without eIFs or $tRNA^{Met}$ [72]. Furthermore, the IRES

elements belong to one of two groups, which differ in sequence, secondary structure, and the location of the translational initiation codon [58]. The first functional region consists of a highly conserved 5’ terminal cloverleaf encompassing domain I as well as an adjacent pyrimidine rich single stranded sequence. This region is required for positive and negative strand synthesis during viral genome replication [53, 59, 60], whereas the other functional region is composed of domains II–VII that make up the IRES. In 1988, Pelletier and Sonnenberg found that due to the lack of a 7-methyl guanosine cap structure found in eukaryotic mRNA, the IRES of CVB3 RNA instead interacts with the host cell ribosomes directly to initiate translation of the viral genome [61] determining CVB3 to have a type 1 IRES (Figure 3). The IRES, regardless of type, is responsible for initiating cap-independent translation in picornaviruses [53, 61]. Importantly, in addition to coding regions, virulence determinants have been identified within the 5’ UTR of CVB3 genome. The generally accepted mechanism for 5’ UTR-dependent virulence attenuation is an introduced mutation or accumulation of mutations that disrupt the critical RNA secondary and tertiary structures in that region. Such structural alterations confer inefficiencies in viral processes such as genome replication and cap-independent translation [53, 62, 63].

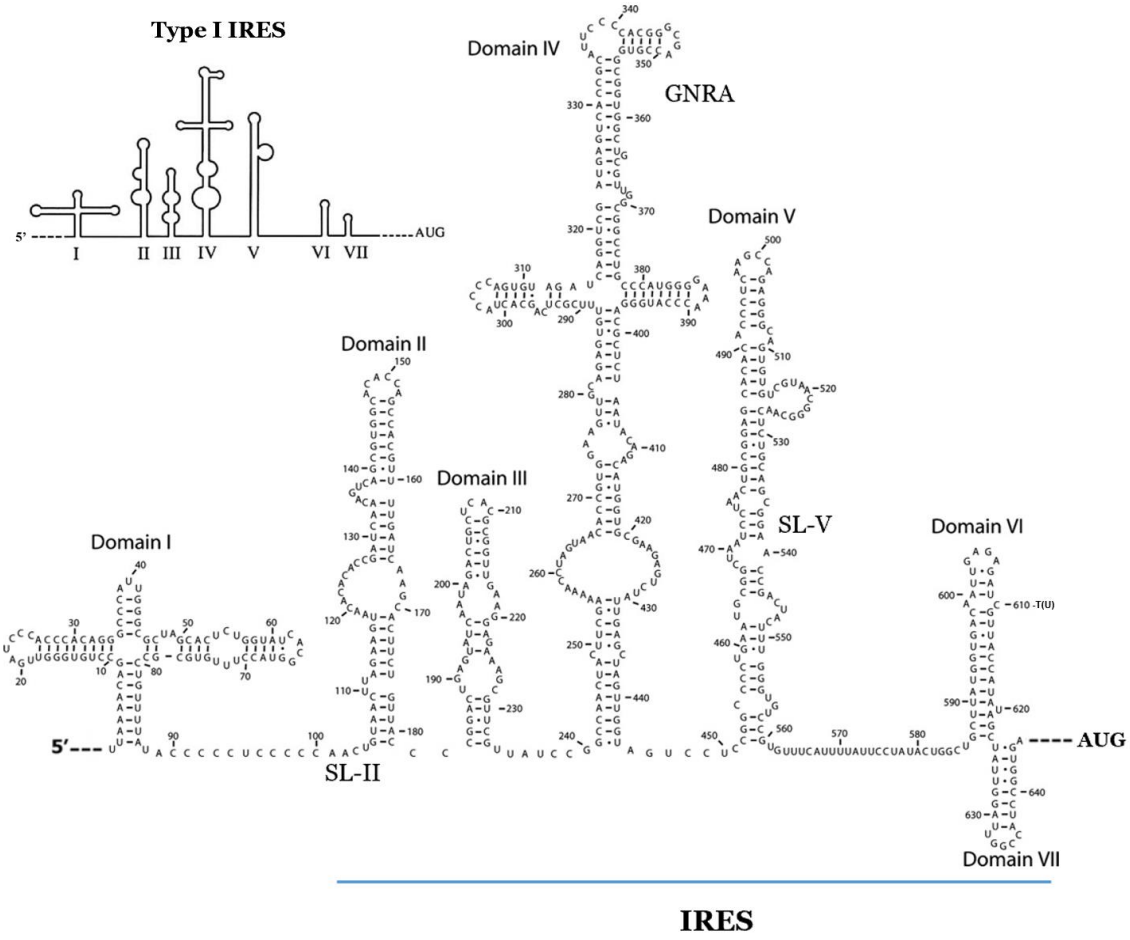

Figure 3: Schematic representation depicting the Coxsackievirus 5' UTR. Top: General outline of the type I IRES adapted from Dunn, J. et al., (2002) Bottom: 5' UTR of the CVB3 genome: Secondary structure model of domains II-VI labeled. GNRA, SL-II and SL-V as well as type I IRES are present in the 5' UTR of the CVB3 genome. Mutation C610T(U) found in the 5' UTR of the CVB3/IC genome shown. Nucleotide sequence shown is that of CVB3/28 and adapted from Bailey & Tapprich (2007).

Seeking to characterize the 5' UTR *in vivo,* research conducted by Zhewei Liu et al. identified the most crucial region of the IRES as a 46-nt pyrimidine-rich segment spanning from nts 546 to 592 between stem-loops G and H and additionally identified a second crucial region in the proximate 5' end of the 5' UTR [64]. Lui and others found that deletion of this segment could abolish viral infectivity but not protein translation. Furthermore, Lui and his team were the first to suggest that the 5' UTR of picornaviruses harbor *cis* and *trans*-acting sequence elements vital for viral translation and infectivity.

Resulting in decreased translation [65], a point mutation found at nt 472 correlates with attenuated poliovirus type 3 neurovirulence in vivo, clearly linking viral translation efficiency with viral virulence [64, 66]. Additionally, a point mutation found at nt 234 of CVB3 RNA has been associated with reduced viral cardio-virulence [67], although it was unclear at the time whether the mutation resulted in the down regulation of viral protein translation [64].

Resulting research throughout the years has sought to further describe the 5' UTR of CVB3 and identify viral phenotypes associated with mutations in that region. As previously stated, during viral infection the 5' UTR takes part in a series of events that ensure efficient viral gene expression and replication with translation and replication controlled by different 5' UTR RNA domains (Figure 3). Whereas domain I, encompassing a highly conserved cloverleaf structure, directs the replication of both positive and negative strands [59, 68], domains II-VII work together to form the critical IRES that controls translation [68].

As myocarditis poses a significant health threat to many worldwide, determining areas of the CVB3 cardio-virulence becomes vital. Research conducted by Dunn et al. confirmed the single nucleotide in the CVB3 5'UTR at position 234 within domain III as the determinate of cardio-virulence [53, 67]. Notably, the region connecting domain I and domain II combined with domain II at positions 88-181 in the CVB3 5'UTR has been commonly referred to as stem loop II (SLII) [69], a region found in other EVs and identified as a virulence determinant [70, 71]. Exchanging the naturally occurring avirulent CVB3/CO SLII region with the virulent CVB3/AS strain, Dunn et al. showed that cardio-virulence in a murine model follows SLII of CVB3/AS and further that

cardio-virulence could be conferred to infectious CVB3 clones following SLII mutation (Figure 3) [71].

As technology continually progressed, further insights into the SLII region have been illuminated. In 2000, Lee et al. employed theoretical RNA folding algorithms and sequence comparison analysis to characterize and predict an altered secondary structure found in the SLII region of the non-cardio-virulent CVB3/GA in comparison to cardio-virulent CVB3 strains [53, 63]. These theoretical approaches proved useful in repeatedly predicting secondary structure differences in virulent and avirulent 5' UTR regions with CVB3 where the primary sequences were not conserved, including those in the CVB3 SLII [63, 70, 71] and at the time further strengthened the proposed model that structural alterations in SLII underlie changes in CVB3 virulence phenotypes [53].

Later, Prusa et al. compared the 5'UTR structure of the avirulent CVB3/GA strain with the virulent CVB3/28 strain using chemical probing analysis [53]. Although Prusa et al. confirmed a SLII structural difference between CVB3/28 and CBB3/GA, the probing analysis did not match the structural alteration predicted by energy minimization. In contrast to Lee et al., Prusa et al. exchanged the SLII region (nt 104–184) between CVB3/GA and CVB3/28 and repeated chemical probing analysis of the full length 5'UTR with the chimeric constructs [53]. When the full length naturally folded 5'UTR of CVB3/GA and CVB3/28 were compared, substantial structural alteration in the SLII region could be observed. In the end, Prusa et al. found CVB3/28 SLII exhibited pairing between positions 128–132 with 162–166 forming a lower stem, a structure absent in CVB3/GA [53]. Significantly, the chemical probing analysis demonstrated that the secondary structure of SLII followed the parent molecule rather than depending on the

5’UTR structures outside of the SLII region suggesting that the 5’UTR structural domains fold independently (Figure 3). These results coupled with others confirm that the CVB3 SLII is both structurally and functionally independent as a cardio-virulence determinant [53, 58].

Other areas within the 5’ UTR of CVB3 have shown to play an essential role in viral virulence. For instance, Bhattacharyya et al., investigated the influence of the conserved hexa-nucleotide stretch (nt 104–180) located in the apical loop within stem-loop C (SL C) on CVB3 IRES function. The results clearly demonstrated that a deletion or substitution mutation within the apical loop resulted in a nearly 50% decrease in IRES activity. Interestingly, the study found that the mutant IRES RNA failed to interact with certain trans-acting factors within the 5’ UTR [62]. The research also found that expression of the CVB3 2A protease significantly enhanced IRES activity of the wild type CVB3 but exerted little effect on mutant IRESs in the study. This finding led researchers to conclude that the particular mutant RNAs found in the 5’ UTR were unable to interact with some trans-acting factors critical for enhanced IRES function. Despite the substitution mutation, however, the local structure of the IRES RNA was not significantly altered implying the SL C/c apical loop structure is highly conserved and therefore likely plays a critical role in CVB3 IRES function [62].

Further investigations into stem-loop structures located in the CVB3 5’ UTR have proven fruitful. The stem-loop V (SL-V) of the CVB3 IRES contains a large lateral bulge loop encompassing two conserved GNRA motifs [72]. Conferring exceptional stability to RNA structure, the tetraloop motif is a four-base hairpin loop motif found in RNA secondary structure that functions to cap double helices. The GNRA tetraloop has a

guanine-adenine base-pair where the guanine is 5' to the helix and the adenine is 3' to the helix (Figure 3). As structural elements, GNRA motifs are believed to be involved in reorganization of RNA structure through long-range RNA-RNA interactions [73]. Additionally, research has shown that the 3’ terminal adenine residue of the GNRA loop in encephalomyocarditis virus is critical for function [74] and mutational analysis revealed that virus IRES activity for hand, foot, and mouth disease depends on the integrity of the GNRA loop [74].

Ben M’hadheb-Gharbi et al. went on to further characterize the importance of the GNRA loop in the CVB3 5’ UTR. Analyzing the effects of point mutations within the GNRA motifs of the CVB3 IRES, Ben M’hadheb-Gharbi et al., characterized in vitro virus production and translation efficiency and further tested in vivo virulence of two CVB3 mutants. The study found that both mutant RNAs displayed decreased translation initiation efficiency when translated in rabbit reticulocyte lysates. Additionally, yields of infectious virus particles in HeLa cells decreased in the mutant RNA when compared with the wild type. In vivo, both mutant viruses were avirulent and caused neither inflammation nor necrosis in hearts suggesting translation initiation is highly influenced by GNRA motifs within the SL-V of the IRES of CVB3 [75].

2.3 Sabin-like PV mutations in the CVB3 genome

The scientist best known for his development of the first oral polio vaccine, Albert Sabin identified attenuated strains of each Poliovirus (PV) serotype which were unable to productively infect and destroy neuronal cells [76]. While several mutations distinguish the virulent and attenuated PV strains, many playing a direct role in neurovirulence, the vaccine strain of each PV serotype employs an attenuating mutation

found in the PV 5' UTR. Interestingly, these attenuating mutations are identified at a position very near to each other within SL-V of the IRES (nucleotides 472, 480, and 481 respectively for PV Sabin 3, 1, and 2) [77]. Eventually, experimental evidence led to the conclusion that the major mutation sufficient to induce the principal characteristics of attenuation was indeed the mutation in the PV 5' UTR [78, 79]. Due to the genetic similarities shared between PV and CVB3, Ben M'hadheb-Gharbi et al. hypothesized that Sabin-like mutations generated in the 5' UTR of CVB3 may produce similar results and therefore lead to an effective vaccine for CVB3.

Following the insertion of three Sabin-like attenuating mutations into CVB3-Nancy IRES region equivalent, Ben M'hadheb-Gharbi and his team found that only the Sabin3-like mutation led to serious perturbations in translation efficiency, virus titer and/or secondary structure [80]. Whereas the Sabin3 mutation in PV1 results in partial destabilization of the secondary RNA structure of domain V within the IRES [78] causing a reduced recognition of this region by protein factors necessary for PV translation initiation, biochemical probing of the secondary structure of the entire domain V of the IRES of Sabin-like mutants revealed no distinct profiles in comparison with the wild-type counterpart [80].

To test whether a single change in the sabin3-like CVB3 mutant could recapitulate the attenuating effect seen in in the vaccine PV1(M) strain, Ben M'hadheb-Gharbi et al. subsequently supplemented one mutation (U475 → C) in the CVB3 mutant carrying the Sabin3-like mutation. The study revealed that when introduced together into the CVB3 genome the U475→C plus Sabin3-like mutations resulted in a greater decrease in viral titer and translation efficiency when compared with the effect of the CVB3

Sabin3-like mutation alone. Additionally, the modified mutations produced viruses with increased growth kinetics defects when compared to that of Sabin3-like mutant viruses and importantly, both IRES mutants demonstrated little or no disease in hearts of orally infected mice [77]. Taken together, these results suggest that specific protein-viral RNA interactions are disrupted thereby preventing efficient viral translation.

Finally, Ben M'hadheb-Gharbi et al. used a proteomic approach to identify eIF4G (p220), eIF3b (p116) and eIF4B as potential RNA-binding proteins interacting with domain V. These studies confirmed that the this single-nucleotide (U475→C) exchange impaired the interaction pattern and the binding affinity of the standard translation initiation factors within the IRES domain V in the mutant strain. In all, Ben M'hadheb-Gharbi et al. revealed that Sabin3-like mutations introduced into the CVB3 5' UTR contributed to the attenuation of the cardio-virulence, a reduced translation efficiency, an impaired ribosomal initiation complex 48S and 80S assembly and observed a reduced RNA protein binding pattern within the full IRES sequence impaired binding of the translation initiation factors eIF3, eIF4G and eIF4B to the IRES domain V mutant RNA [81, 82]. These studies provide further evidence for the crucial role of RNA structure for the IRES activity and reinforce the idea of a distribution of function between the different IRES structural domains.

2.4 The role of the CVB3 VP region in virus-host-cell interaction

The open reading frame within the CVB3 genome is divided into three regions referred to as P1, P2, and P3. Encoded within the P1 region, comprising the roughly 29 nm icosahedral viral capsid are the four capsid proteins, VP1-VP4 (Figure 1) [83]. One molecule each of VP1, VP2, VP3 and VP4 makes a protomer, five protomers compose a

pentamer and 12 pentamers complete the viral capsid, in total the capsid is composed of 60 protomers (Figure 4). The outer layer of the capsid is composed of VP1, VP2 and VP3 whereas VP4 is an internal protein [24]. The enterovirus capsid plays an invaluable role in virus-host cell attachment and entry. Critically, the capsid forms distinct topological features as each five-fold icosahedral symmetry axis is surrounded by a depression termed the canyon, where a known receptor binding site is located. Likely a lipid moiety, the capsid also contains a hydrophobic pocket called the "pocket factor" which lies directly beneath the floor of the canyon. Finally, at the southern rim of the canyon, there is an elevated hypervariable region called the "puff" region that is a known antigenic site [17, 84].

To gain entry to the host cell, the canyon region within the viral capsid binds to CAR. Virus-host cell receptor interaction results in the loss of the pocket factor which in turn triggers the virus to transition to the altered particle, or A-particle. Due to the loss of VP4, the subsequent CVB3 A-particle is rendered avirulent and the exposure of the N termini of VP1 results in the inability for the particle to bind to the receptor, however, it has yet to liberate the viral (+)ssRNA genome [85]. Several virulence determinants have been identified in the enterovirus genome in regions encoding the structural capsid proteins VP1–VP4 [53].

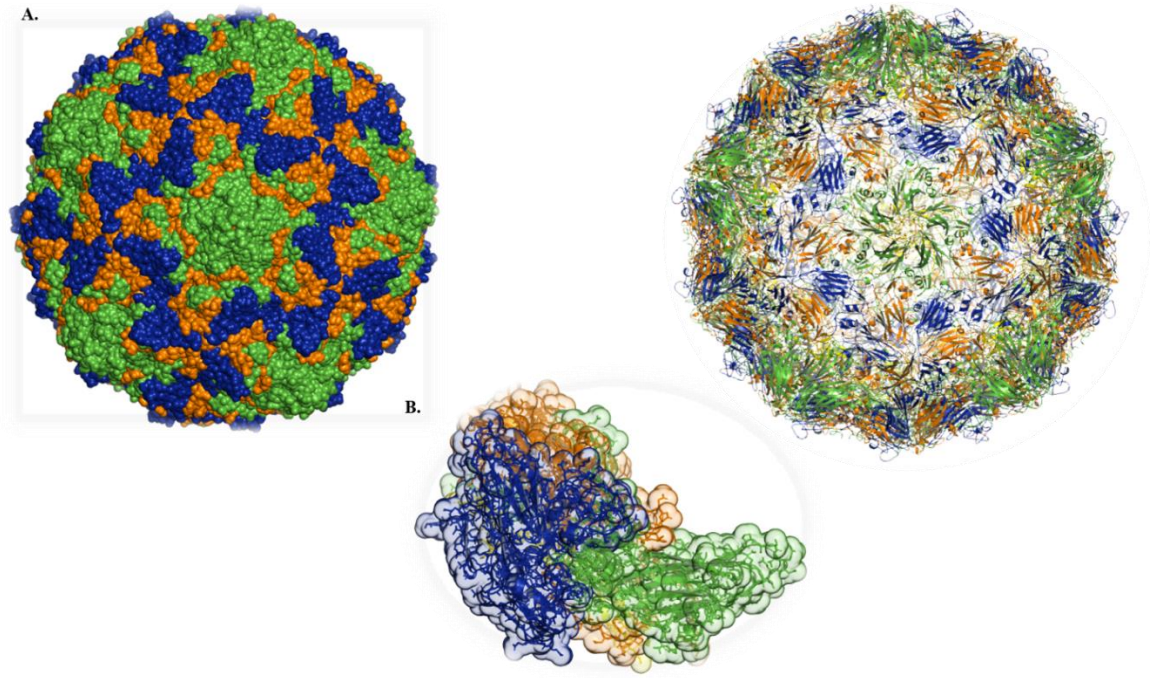

Figure 4: Capsid structure of CVB3 Nancy. (A) The coxsackievirus virion structure showing detailed capsid protein structure as determined using x-ray crystallography. A 5 fold axis of symmetry with its surrounding canyon displayed in the center of the image. (B) CVB3/ATCC capsid pentamer. CVB3 capsid proteins labeled VP1-green; VP2-blue; VP3-orange. The image was generated using PyMOL (2.3.4) and publicly available data provided by Muckelbauer, JK and Rossmann, MG obtained from rscb.org protein databank.

2.5 Capsid VP region and viral virulence

Among enterovirus' there is also strong evidence that the structural genes affect both tissue tropism and virulence. For example, mutations in both the VP1 and the VP4 structural genes have been shown to modulate the virulence of CVB4 for pancreatic tissue while poliovirus attenuation is associated with mutations in VP1, VP3, and VP4 as well as the 5' UTR [86]. Additionally, Caggana, M., P. Chan, and A. Ramsingh, identified several amino acid substitutions within the VP1, VP2, and VP4 capsid proteins of virulent CVB4 correlating the major determinants of virulence to a single amino acid Thr-129 in VP1 [87].

Describing a viral mutant derived from a cardio-virulent strain of CVB3, Zhang et al., sought to delineate the mechanisms conferring attenuated virulence and a large plaque phenotype. Following sequencing of the VP3 and VP1 regions of the attenuated CVB3 mutants, three nucleotide changes were identified in the VP1 coding region. The mutations included a silent single base change at nucleotide position 2467 (C to U) and a double-base change at position 2690-1 (AA to GT). The latter lead to a change from lysine to serine at amino acid position 80. Zhang and his team, concluded that the VP1 mutation serine-80 in was in fact a determinant of the large plaque phenotype but was not responsible for virulence attenuation [88].

With the goal of extrapolating the determinant of CVB3 cardio-virulence, Knowlton et al. compared the full genome sequences of a cardiotropic variant of CVB3/H3 and an antibody escape mutant H310A1 capable of attenuating the cardio-virulent potential of the virus in mice despite ongoing viral replication in the heart. Comparison of the two variants revealed a single non-conserved mutation (A to G) in the P1 polyprotein region at nucleotide 1442 resulting in an asparagine-to-aspartate mutation in amino acid 165 of VP2 corresponding to the puff region in that area. Importantly, it was shown that the presence of asparagine at amino acid 165 of VP2 was associated with the cardio-virulent phenotype, whereas an aspartate at the same site markedly reduced cardio-virulence potential. Additionally, BALB/c mice infected with a CVB3 mutant containing the VP2 asp165 mutation displayed high levels of TNF-a secreted by monocytes. These data suggest that a point mutation in the puff region of VP2 may alter the ability of CVB3 to induce myocarditis in BALB/c mice and stimulate the production of TNF-a secretion from infected BALB/c monocytes [89].

Further characterizing the role of VP1 in viral pathogenesis, Schmidtke, M., et al. conducted in vitro studies to examined the phenotypic results caused by six unique amino acid substitutions in the VP1 capsid protein found between the CVB3 strains Nancy P (CVB3/P) and the derivative variant PD (CVB3/PD). While CVB3/P can establish a persistent carrier-state infection absent visible cytopathic effect in primary human fibroblasts (HuFi H), CVB3/PD, a CVB3 variant that uses heparan sulfate as a receptor to infect CAR-negative cells, induced complete lysis of the cell monolayer. After comparing CVB3/P and CVB3/PD genomes with published CVB3 sequences, mutational analysis revealed that amino acid residues K78, A80, A91, and I92 in VP1 were necessary to induce lytic infections in HuFi H cells. Schmidtke, M., et al. further demonstrated that CVB3/P preferentially bound CAR, while the CVB3/PD exhibited a weak interaction with CAR but a strong binding affinity for DAF [90, 42]. The in vitro data suggest that specific mutated amino acid residues in VP1 are involved in receptor recognition/binding. Further, the study suggests lytic replication of CVB3/PD in various non-permissive rodent cell lines indicates VP1 may exert influence on viral ability to bind to cell surface molecules other than CAR and DAF (Table 1) [90].

To delineate determinants of viral virulence for the heart and pancreas, Stadnick et al., identified ten CVB3 antibody escape mutants. The generation of these mutants was then used to determine the integral nucleotide substitutions involved in immune evasion. Stadnick et al., sequenced the P1 region of each escape mutant and isolated mutations associated with the lack of neutralization, finding eight of the ten escape mutants harbored a lysine-to arginine mutation in the puff region of VP2. The other two mutants, meanwhile, exhibited a glutamate-to-glycine substitution in the knob region of VP3.

Upon further sequencing and analysis, two viral mutants representing a lysine-to arginine mutation and glutamate-to-glycine substitution, EM1 and EM10 respectively, displayed additional mutations. Among them, EM1 displayed two mutations in the region coding for the viral 3D polymerase, while EM10 exhibited a mutation in the previously mentioned stem-loop II of the 5' UTR. Stadnick, et al., proceeded to delineate, via *in vivo* models using A/J mice, the comparative pathogenesis of the mutants relative to that of the parental myocarditic strain, CVB3/RK. The results of the in vivo experiments showed that both escape mutants were less cardiotropic than CVB3/RK, with EM1 and EM10 exhibiting a 40-fold and 100- to 1,000-fold reduction, respectively, in viral titers in the heart compared to CVB3/RK. To confirm the findings, the VP2, VP3, and the 5'NTR mutations were independently introduced into a CVB3/RK infectious clone. The resulting phenotypes following mutation substantiated the reduced cardio-virulence caused by mutations introduced in the VP2 and VP3 regions suggesting that additional mutations in the VP2 and VP3 structural proteins contribute to cardio-virulence attenuation in mice.

2.6 Capsid proteins influence in virus-host-cell binding

As previously mentioned, most known Coxsackievirus isolates utilize CAR as their main receptor to facilitate host-cell entry (Figure 2). In polarized gut-epithelial cells CAR is located within the tight junctions, making the receptor nearly inaccessible to CVB3 [91]. Nevertheless, the accepted origin of infection is within the gut-epithelia, raising the question of how CVB gains access to CAR in the first place. Several studies have confirmed that many CVB serotypes including CVB1, 3, and 5, as well as several other enteroviruses, bind to DAF (CD55, a glycosylphosphatidylinositol (GPI)-anchored

complement regulatory protein), thereby facilitating the shuttling of the virion to CAR in the tight junctions [92-94].

Naturally, the first- DAF-binding CVB isolate (CVB3/RD) was obtained following repeated passaging of the parental CVB3-Nancy in human rhabdomyosarcoma (RD) cells. Whereas RD cells express ample amounts of DAF, they have very little available CAR. Thus, to determine the molecular basis for the specific interaction of CVB3/RD with DAF, Pan et al., produced cDNA clones for both CVB3/RD and CVB3/Nancy and created mutations at each of the sites where the RD and Nancy sequences diverged. Experiments showed a single amino acid change in VP3- E234Q resulted in an increased capacity of CVB3/Nancy to bind DAF in RD cells [92]. Next, Pan et al., examined the RD adaptation in the cardio-virulent CVB3/H3. Whereas the H3 variant that does not measurably bind DAF, it already possesses VP3-234Q. The authors identified a resulting H3 DAF-binding isolate, revealing a second mutation in VP2 (VP2-N138D). Subsequent experiments found mutation of either residue in CVB3/RD resulted in a loss of avidity for DAF, indicating that both VP3-E234Q and VP2-N138D are important for virus interaction with DAF. Interestingly, upon cryo-electron microscopy, both VP3-234Q and VP2-138D were found at the contact site between the virus and DAF [92], further suggesting that mutations in the structural proteins may result in phenotypes with altered binding capacity.

2.7 Capsid proteins impact on viral stability

Not only has it been observed that mutations in the VP region result in altered virulence and cell-binding affinity, but mutations found in VP1 and VP3 have been further implicated in viral stability. As evidence of this phenomenon, CVB3/RD exhibits

increased stability when compared to the virulent CVB3/28 [95]. Due to its primary propagation being restricted to CAR-rich HeLa cells in a laboratory setting where it is not required to survive for very long at 37 °C in the absence of readily infected host cells, it has been proposed that CVB3/28 stability may have arisen from lack of selection pressure. In that vein, when Carson et al. subjected CVB3/28 to selection pressure and analyzed those variants from the CVB3/28 population selected for increased stability at 37 °C, the capsid proteins of the stable variant differed from the parental CVB3/28 by two mutations in VP1 and one mutation in VP3. A single capsid mutation in the VP1 residue Q80K (glutamate to lysine) was observed in the more stable CVB3/28. Located near the apex of the fivefold prominence, VP1 residue 80 is proximal to VP1 residues 78 glutamate, 85 lysine, 86 arginine and 230 lysine, therefore the mutations effects on stability may be explained by the exchange of a negatively charged glutamate with the ability to participate in ionic interaction with the three nearby positively charged side chains, with the positively charged lysine. A lysine at VP1 residue 80 may contribute to a positive charge cluster resulting in increased capsid interaction with anionic secondary ligands [85]. The observed VP3 A180T mutation (alanine to threonine) was found to lie in the canyon that surrounds the fivefold axis of symmetry. In the event that alanine is exchanged with threonine, it is hypothesized that the expected hydrophobic interaction with the residue 146 proline in VP1 of the adjacent protomer would have the potential to contribute an additional hydrogen bond to the adjacent VP1 backbone thereby strengthening inter-protomer binding, affecting receptor binding and capsid expansion.

Additional information gleaned from further experiments performed by Carson et al. suggest that mutations found in VP1-92 could determine whether the virus exhibited

low stability (CVB3/28) or high stability (CVB3/28N). Amino acid 92 is located in the hydrophobic pocket of VP1 where the stabilizing lipid, called the pocket factor, and stabilizing antiviral compounds are bound [17, 96, 97]. In separate studies, leucine at VP1-92 was associated with CVB3 resistance to pleconaril, an antiviral drug that inhibits picornavirus replication by binding to a specific hydrophobic pocket within the viral capsid and preventing viral attachment or uncoating of the genome [98]. Due to the importance of the pocket in the conformational capsid breathing, Carson et al., established a key determinant of virus stability at the VP1 residue 92 [85].

Finally, Wang and Pfeiffer identified a single amino acid change in VP3 N63Y that, following in vivo passage, resulted in a viral mutant that produced a large-plaque phenotype. Following oral inoculation of CVB3/Nancy, feces collected from mice and subject to plaque assay exhibited plaques >100 times as large as inoculum viruses upon Hela cell using an agar overlay. When an agarose overlay was substituted for agar, however, both the wild-type CVB3 and N63Y mutant CVB3 resulted in similar plaque sizes. Wang and Pfeiffer further determined that sulfated glycans in agar inhibited plaque formation by wildtype CVB3 but not by N63Y mutant CVB3 and that the N63Y mutation resulted in a reduced ability to bind heparin, a sulfated glycan. Significantly, while the VP3 mutation exhibited a growth defect and reduced attachment in cultured cells, it displayed enhanced replication and pathogenesis in mice. Furthermore, the studies demonstrated that infection with N63Y mutant CVB3 induced more severe hepatic damage than infection with wild-type CVB3 adding evidence to the notion that, due to the lack of selection pressures, culture-adapted laboratory virus strains may have reduced fitness in vivo [99].

2.8 Non-structural mutations found in the CVB3 genome

As noted above, several studies have reported nucleotide sequence differences in within the CVB3/Nancy 5' UTR corresponding with varying degrees of disease severity as such research has primarily focused on mutations occurring within the 5' UTR as well as those found in VP coding regions. Mutations observed in the encoded P2 and P3 non-structural regions, however, are scarce. Indeed, mutations found in the P2/P3 region generally do not confer alterations in pathogenicity or virulence.

One study conducted by Massilamany et al., identified three novel nucleotide substitutions that differed from the parental CVB3/Nancy strain including a single nt change from C5088U resulting in P1449L in non-structural protein 3A. The two other observed mutations were a silent mutation at position C97U in the 5' UTR as well as at position A4327G in non-structural protein 2C. Interestingly, in vivo experiments conducted in the different mouse strains showed that the disease-inducing ability of the infectious clone-derived virus was restricted to pancreatitis alone, and the incidence and severity of myocarditis were significantly reduced. Following reversal of the observed nt mutations Massilamany et al., found the resultant viral titers comparable to CVB3/Nancy. The virions derived from the third clone, however, induced myocarditis comparable to that of the wild type virus while the pancreatitis-inducing ability remained unaltered. As evidence by the selective attenuation of cardio-virulence but stable pancreatitis observed in the C97U and C5088U mutants, this study suggests that the occurrence of mutations within the non-structural coding regions of the CVB3/Nancy genome can differentially contribute to viral virulence by organ type. The availability of such tools may permit us

to determine the molecular mechanisms of differential organ specific disease phenotypes in future studies [100].

In summary, while mutations in the 5' UTR have been conclusively linked to cardio-virulence, several studies support the claim that mutations in the structural proteins may also play a significant role. Whereas mutations found within the 5'UTR of various CVB3 strains logically play a substantial role in determining strain virulence, structural proteins have been observed as major determinants of tissue tropism as well as viral stability. In addition to these well-established determinants, it is possible that nonstructural genes also play key roles in the ability of a virus to propagate in different cell types [86, 100].

2.9 CVB3 models of disease

Due to its prevalence, pathogenesis, and vast genetic variability, CV stands as an incredibly relevant enteric virus model. Accordingly, a range of CV viral genotypes and CV strains that infect mice have been identified in studies observing enteric virus pathogenesis. In addition to pathogenesis studies, various CV variants are used to faithfully induce important disease state phenotypes such as DCM and myocarditis within the different mouse strains (C57BL/6, B10.D2, BALB/c, DBA/2, A/J or C3H/HeJ). In addition to models of CVB3-induced myocarditis, non-obese diabetic (NOD) mice develop spontaneous autoimmune diabetes similar to human T1D have proven instrumental in research concerning the susceptibility, diabetogenesis, tropism and mechanisms of pancreatic [β] Î²-cell destruction in the context of CVB infection [101]. While A/J or C3H/HeJ animals display high susceptibility to CVB3-induced myocarditis [24, 102], least vulnerable to CVB3 infection are C57BL/6 mice.

Whereas WT C57BL/6 mice display susceptibility to intraperitoneal (IP) injection of CVB3, oral inoculation of these mice prove difficult. To facilitate in vivo studies of CVB3 mice deficient in the interferon a/b receptor ($IFNAR^{-/-}$ mice) can be useful. Following CVB3 oral inoculation, $IFNAR^{-/-}$ mice exhibit increased viral titers as well as increased mortality [36]. It is critical to note that while organ systems in various mouse models have been shown to be susceptible to CVB infection, many rely upon intraperitoneal injection to observe pathophysiology.

CHAPTER THREE

3. Materials and Methods

3.1 Mouse experiments

Animal work was performed in accordance with Indiana University School of Medicine IACUC-approved protocols. All procedures and practices were in compliance with the Animal Welfare Act regulations, the Institution's NIH Assurance Statement and any other regulations or policies that apply. Mice were handled according to the Guide for the Care and Use of Laboratory Animals endorsed by the National Institutes of Health. All mouse studies were performed at IU School of Medicine using protocols approved by the local Institutional Animal Care and Use Committee in a manner designed to minimize pain, and any animals that exhibited severe disease were euthanized immediately with carbon monoxide.

Wild type C57BL/6 PVR and C57BL/6 PVR IFNAR−/− mice were obtained from Julie Pfeiffer (University of Texas Southwestern, Dallas, Texas). For oral inoculations, 10- to 12-week-old mice were perorally inoculated with 5×10^7 PFU of CVB3-Nancy. Disease was monitored until day 14 post-inoculation for survival experiments. In the event of severe disease onset mice were euthanized. For shedding and replication experiments, feces was collected at varying timepoints and processed for plaque assay or RNA extraction. For tissue titers, heart, liver, kidney, spleen, small intestine and large intestine were aseptically removed.

3.2 Cells and viruses

HeLa cells were propagated in Dulbecco's modified Eagle's medium (DMEM) supplemented with 10% calf serum, 1% penicillin-streptomycin, 1% amphotericin and

maintained at 37°C, 5% CO_2. Human colorectal carcinoma cells were obtained from ATCC (ATCC® CCL-247) and maintained in McCoy's 5A (modified) Medium supplemented with 10% calf serum, 1% penicillin-streptomycin, 1% amphotericin at 37°C, 5% CO_2. Human Coxsackievirus B3 Nancy strain was obtained from ATCC (ATCC® VR-1034AS/HO), and the CVB3-Nancy infectious clones were obtained from Julie Pfeiffer (University of Texas Southwestern, Dallas, Texas). Stocks of CVB3 were prepared in HeLa cells by co-transfection of the infectious clone plasmid and a plasmid expressing T7 RNA polymerase.

3.3 Sequence analysis and phylogenetic tree construction

For sequencing of CVB3 variants, permissive HeLa cells were infected with the respective virus and used for RNA preparation according to the method of Chomczynski and Sacchi (1987). A 5-mg sample of the total RNA was reverse-transcribed. The resulting cDNA was PCR-amplified with the Superscript II (ThermoFisher^{TM}) and DNA fragments were sequenced, employing a set of 13 DNA primer pairs (not shown). The GenBank accession numbers are: AY673831 (CVB3 GA), AY752944 (CVB3 28), AY752945 (CVB3 0), AF231763 (CVB3 31-1-93), AF231764 (CVB3 P), AF231765 (CVB3 PD), M88483 (CVB3 20), KC481610 (AH30), JN048469 (CVB3 RD), KJ025083 (CVB3 MKP), JX843810 (CVB3 A103/KM/09), M16572 (CVB3-Nancy), and (CVB3 H3 Woodruff variant).

Whole genome sequences of 12 known CVB3-Nancy strains were downloaded from the National Center for Biotechnology Information (NCBI). Nucleotide and amino acid sequences analysis and sequence identity comparison with other CVB3 serotypes from GenBank were completed by NCBI BLAST and MEGA-X software (citation

needed). The phylogenetic tree was constructed using polyprotein amino acid sequences aligned with MUSCLE [103, 104]. The evolutionary history was inferred by using the Maximum Likelihood method and JTT (Jones-Taylor-Thornton) matrix-based model, the tree with the highest log likelihood is shown. RNA secondary structure was predicted by the MFOLD program (http://mfold.rna.albany.edu/). The structure was modified from a previously determined crystal structure (Protein Data Bank code 1cov) [105].

3.4 Plaque assay

HeLa cells were plated in six well plates and incubated at 37°C with 5% CO_2 overnight, at which time they reached ~70-90% confluency. Feces from infected mice were resuspended in 1-5 volumes of phosphate buffered saline (PBS) and freeze-thawed 3 times in liquid nitrogen. The suspension was separated by centrifugation at 20,000 rpm for 5 minutes, supernatants were extracted with 10% chloroform to eliminate bacteria, and samples were subjected to centrifugation for 3 minutes. Infectious supernatant was removed and serially diluted in warm DMEM. For organ tissue, the weight of each frozen organ sample was determined, then the tissue was homogenized in PBS, subjected to centrifugation, supernatant was removed and virus chloroform extracted. The resulting supernatant was used for 10-fold serial dilutions prepared in no serum DMEM. Media was aspirated from the 6 well plates, and 200 µl of each serial dilution was added to individual wells. Plates were incubated at 37°C for 30 minutes. Following incubation, virus was removed and replaced with a 1% agar overlay in 1x DMEM. At ~48-72 hours post-infection agar plugs were removed. The monolayers were stained with 1% crystal violet in 20% ethanol, rinsed with DI water, and plaques were

counted. The titer (pfu/g of organ) was calculated based on the weight of each tissue sample.

3.5 One-step growth cycle

One-step growth analysis was performed on HeLa and HCT-116 cell monolayers in 12-well plates at 37°C. Cells were infected with wild-type CVB3-Nancy obtained from ATCC or the CVB3-Nancy infectious clone at a MOI of 10 for 30 minutes at 37°C. Following incubation, cells were washed three times with PBS, and DMEM supplemented with 10% newborn calf serum, 1% p/s, and 1% amphotericin was replaced and the cells were left to incubate at 37°C. Supernatants and cells were harvested together at 0, 2, 4, 6, 8, and 16 hours post-infection (h.p.i). The number of PFU/mL present at each time point was determined by plaque assay.

3.6 Measurement of cytopathic effect (CPE)

Quantification of CPE in HeLa and HCT-116 cell monolayers was conducted using Trypan blue dye to discern between viable and non-viable cells. HeLa and HCT-116 cell were seeded 24 hours prior to the experiment and grown to ~90%-100% confluency. Cell were infected with CVB3-Nancy ATCC strain or CVB3-Nancy IC strain and allowed to incubate for 30 minutes at 37°C. Supernatant was removed and replaced with DMEM supplemented with 10% newborn calf serum, 1% p/s, and 1% amphotericin and left to incubate for 2-3 days. Following infection, cells and serum were collected together and a 1:1 dilution of the cell suspension was prepared in Trypan Blue dye of an acid azo exclusion medium by using a 0.4% Trypan Blue solution. The ratio of non-viable cells (stained blue) and viable cells (unstained) was determined by hemocytometer. Cells were counted under the microscope in four 1 x 1 mm squares of one chamber and

the average number of cells per square determined. Uninfected wells were used as a control.

3.7 MTT reduction assay

HeLa and HCT-116 cell viability was further determined via MTT (3-(4,5-dimethylthiazol-2-yl)-2,5-diphenyltetrazolium bromide) tetrazolium cell viability assay (ATCC® 30-1010K). Following CVB3-Nancy infection at MOI 10 as previously described, cells were incubated for 24 hours or until CPE was observed. Each well received 10 mL MTT reagent and incubated at 37°C for 2-4 hours until purple precipitate was visible. Detergent reagent was then added to cells and the cells were left to incubate in the dark at room temperature for 2 hours. Following incubation, absorbance was read at 570 nm. Several wells were left blank for reference and uninfected wells were used as a control.

3.8 Quantitative real time reverse transcription PCR (qRT-PCR)

Total cellular RNA was extracted from CVB3-Nancy infected HeLa cell monolayers or collected mouse tissues were harvested following a 2-3 day incubation using TRIZOL reagent (Invitrogen, Carlsbad, California, United States) according to the manufacturer's instructions. To measure the relative levels of viral RNA, qRT-PCR targeting CVB3 VP1, and the housekeeping gene β-Actin was performed according to PowerUp™ SYBR™ Green Master Mix (ThermoFisher Scienitific, A25742) manufacturer guidelines. The primer pairs used for viral RNA measurement are as follows: CVB3 VP1 (forward, 5′ AGGAATTCATGGAAGACGCGATAAC 3′; reverse, 5’TGTCTAGATGCTTTGCCTAGTAGTG 3′) and human β -Actin (forward primer, 5’

GCACCACACCTTCTACAATG 3'; reverse primer 5' TGCTTGCTGATCCACATCTG 3'). The CVB3 VP1 gene level was first normalized to β -Actin mRNA, and then to cell numbers.

3.9 Immunohistochemical staining

Protein was extracted from virus-infected or tissue infected cells using ice-cold Radioimmunoprecipitation assay buffer (RIPA) and protein concentration was determined via Bradford. Equal amounts of protein were analyzed by SDS-PAGE, using standard 12% SDS-PAGE gel. Proteins were transferred to 0.2 μm nitrocellulose membranes and blocked with 3% BSA in Tris-buffered saline with Tween 20 (TBST) buffer. Immunohistochemical staining was performed using the primary antibody of monoclonal anti-CVB3 capsid protein VP1 (1:1,200, Cox mAB 31A2, Mediagnost, Germany). Immunoblots were imaged and analyzed on a LI-COR imager.

3.1.1 Tissue titers

Following oral inoculation of $5x10^7$ PFU/mL CVB3-Nancy, mice were euthanized 24, 48, or 72 hpi with CO_2 gas. Immediately following euthanasia the heart, liver, kidney, spleen, as well as serum and intestine were aseptically removed from mice. Each organ was divided into two approximately equal portions, one of which was placed into a cryotube and snap-frozen with dry ice, the other portion of each organ was fixed in 10% normal buffered formalin and processed for histological analyses. Three-micron paraffin sections were prepared and stained with Hematoxylin and Eosin Stain. Tissues snap frozen tissue samples were thawed and homogenized in phosphate-buffered saline using 0.9- to 2.0-mm stainless steel beads in a Bullet Blender (Next Advance). Cellular debris was removed by centrifugation at 12,000 × g for 10 min at 4°C, bacteria was

removed via chloroform extraction and CVB3 was quantified by plaque assay on HeLa cells.

3.1.2 Histology and analysis

Organs were fixed in 10% neutral buffered formalin, sectioned, and stained with hematoxylin and eosin to assess inflammation. For determining the extent of tissue injury, stained sections were graded blindly for inflammation and necrosis by a licensed doctor of veterinary medicine (DVM), MS, Diplomate ACVP, Anatomic Pathologist II using a scale of 0 to 4 in which 0 represented no tissue injury and 4 representing widespread and confluent inflammation.

3.1.3 Statistical Analysis

All results are expressed as mean ± standard error. Statistical analysis was conducted using one-way ANOVA or an unpaired Student's t test as indicated. A value of $p < 0.05$ was considered statistically significant. All results presented are representative of at least three independent experiments.

CHAPTER FOUR

4. Results

4.1 Sequence analysis

To understand the molecular underpinnings of phenotypic differences observed between two CVB3-Nancy variants, we sequenced the whole genome of both CVB3/ATCC and CVB3/IC using RT-PCR method. Complete genome sequence analysis and comparison of the CVB3/ATCC strain and CVB3/IC strain uncovered 11 single point mutation, six of which resulted in non-synonymous mutations. Other mutations found in the P1 region, two amino acid changes in VP3 [asparagine to aspartic acid at residue 63 and tyrosine to phenylalanine at residue 178] and VP2 [lysine to glutamine at residue166] may also be implicated in phenotypic differences observed between CVB3/ATCC and CVB3/IC (Figure 5).

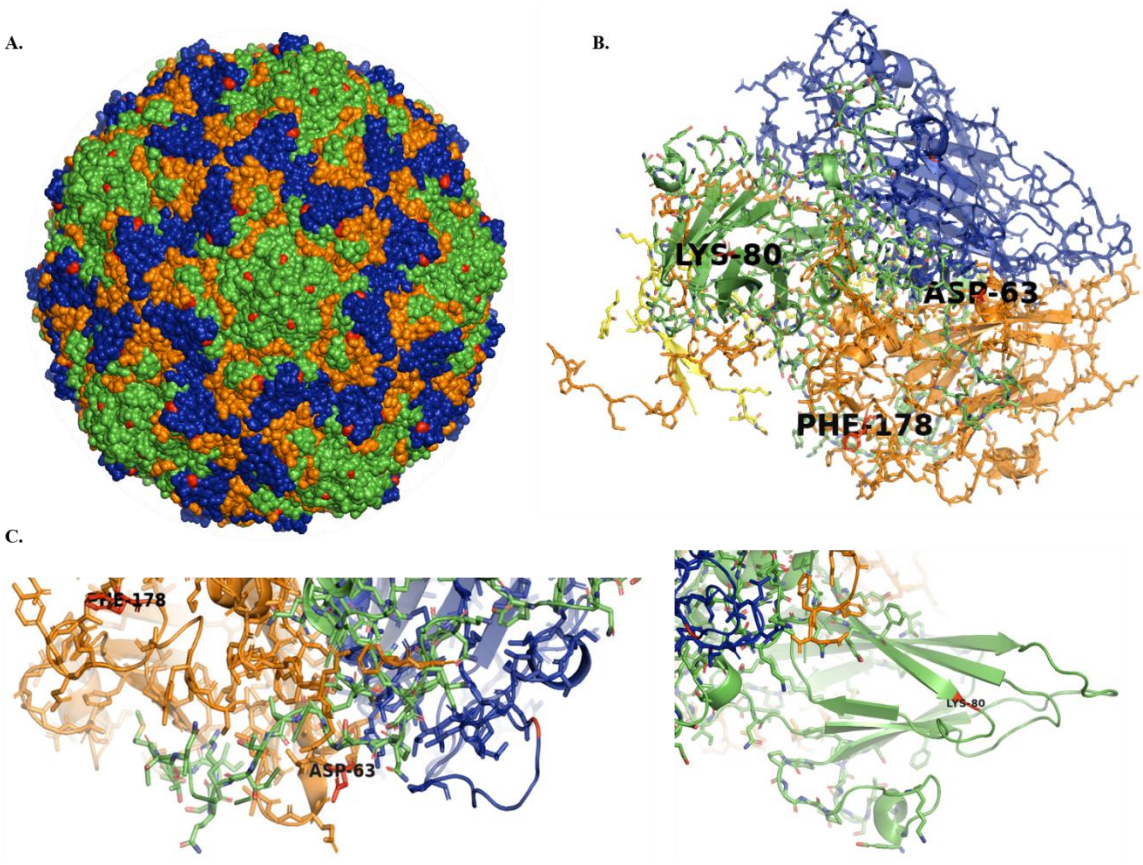

Figure 5: Polymorphisms found in the CVB3/IC capsid structure. (A) The coxsackievirus virion structure showing mutations found in CVB3/IC. (B) CVB3/IC pentamer showing amino acid polymorphisms. (C) VP1 mutation E80K and VP3 mutations N63D and Y178F. Capsid proteins labeled VP1-green; VP2-blue; VP3-orange mutations shown in red. The image was generated using PyMOL (2.3.4) and publicly available data provided by Muckelbauer, JK and Rossmann, MG obtained from rscb.org protein databank.

Following the sequencing of CVB3/ATCC and CVB3/IC, MEGA-X64 was used to create a maximum likely phylogenetic tree. CVB3 Nancy variants with published full-length genome sequences, 11 in all, were downloaded from NCBI for phylogenetic analysis (Figure 6). Phylogenetic analysis of the full length genome sequence of CVB3 Nancy variants with CVB3/ATCC and CVB3/IC show a close evolutionary relationship to CVB3/20. Because mutations found in the VP1 and VP3 region of the genome demonstrated the greatest relevance to viral fitness, these sequences were separately

compared to the corresponding sequences in CVB3/ATCC and CVB3/IC (Figure 6). Analysis of the VP regions revealed a closer evolutionary relationship between CVB3/ATCC and CVB3/MPK whereas CVB3/IC was found to be closely related to CVB3/P and CVB3/0 (Table 1).

A. Full length genome

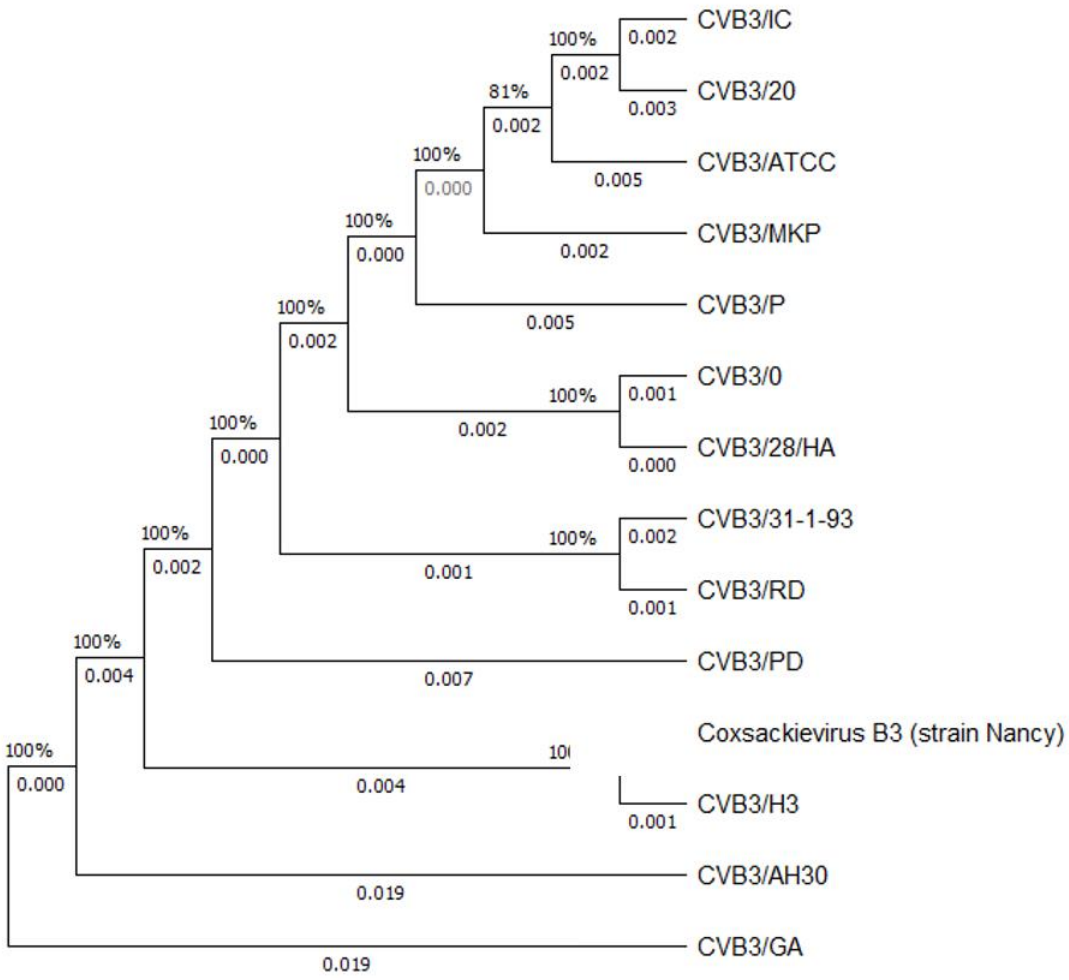

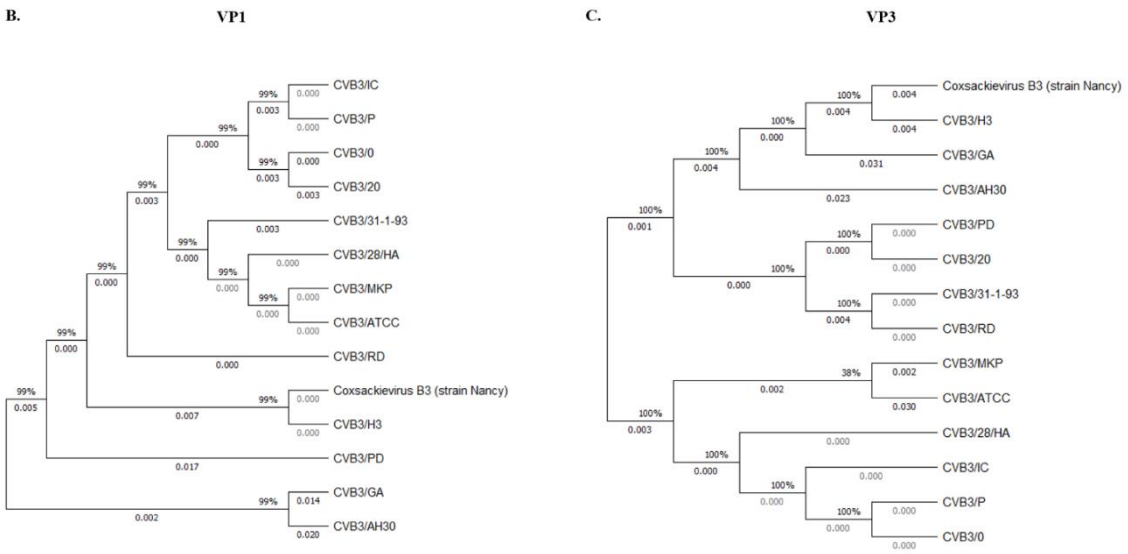

Figure 6: Phylogenetic analysis of CVB3 Nancy variants. (A) Phylogenetic relationships based on aligned fully sequenced CVB3 Nancy amino acid sequences. Trees were constructed separately for VP1 (B), VP3 (C) using the neighbor-joining algorithm implemented in MEGA-X 64 (Kumar et al. 2001).

4.2 CVB3/ATCC exhibits enhanced replication in cell culture

To characterize in vitro phenotypes associated with the two CVB3-Nancy variants, we compared the growth kinetics of CVB3/ATCC and CVB3/IC in HeLa cells. Following in vitro infection of HeLa cells at MOI of 10, samples of virally infected HeLa cells were scrapped into complete media at 0, 2, 4, 6, 8, and 16 hpi. Samples were subject to freeze/thaw 3x and then centrifuged to separate virus from cell debris. Viral replication over time was assessed via standard plaque assay. We found that CVB3/ATCC growth at 4, 8, and 16 hpi was enhanced when compared to CVB3/IC in HeLa cells. To mimic the gastrointestinal environment, we next compared viral growth in the colorectal cell line HCT-116. Simliar to HeLa cells, CVB3/ATCC exhibited increased growth compared to CVB3/IC at 16 hpi (Figure 7). Overall, our data suggest CVB3/ATCC replicates more

efficiently in cell culture and we hypothesized that the replication differences may be the result of altered cell attachment or receptor binding.

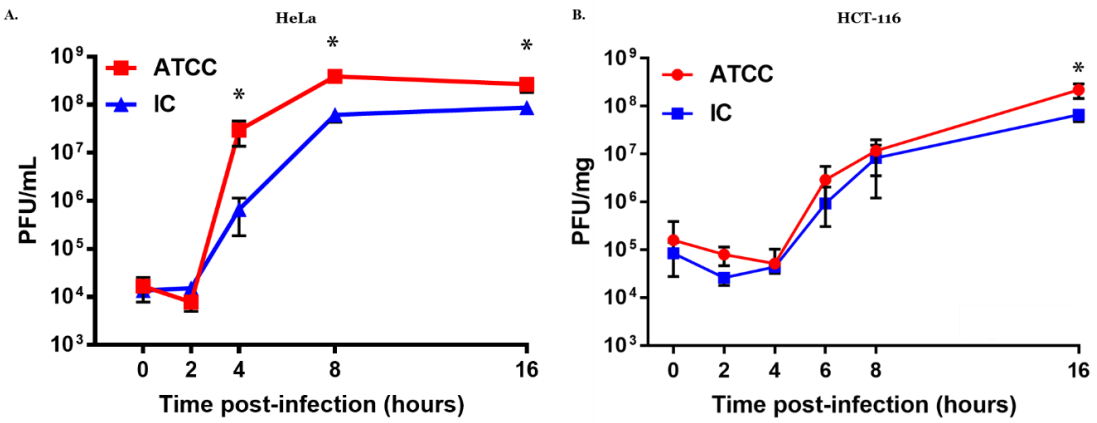

Figure 7: CVB3/ATCC displays enhanced in vitro replication. (A) HeLa and (B) HCT-116 cell monolayers maintained in complete media were inoculated with MOI of 10 of CVB3/ATCC or CVB3/IC virus. Infected cells were scraped from wells and collected at 0, 2, 4, 6, 8, and 16 hpi and subject to plaque assay ($p<0.05$).

4.3 Large-plaque phenotype of CVB3

Mutations mapped to the capsid protein region VP1 have previously been associated with an altered plaque phenotype [99]. We investigated whether mutations observed between our CVB3-Nancy variants conferred a modified plaque morphology. To examine plaque morphology following in vivo infection, virus was extracted from feces collected from orally inoculated CVB3/ATCC or CVB3/IC infected IFNAR-/- mice at 24, 48, and 72 hpi and quantified via plaque assay. The resulting plaques observed following crystal violet staining revealed a much larger plaque size in CVB3/ATCC infected HeLa cells (Figure 8). On average, plaques generated from CVB3/ATCC infected feces were three times larger in area (mm) than the CVB3/IC counterpart every time point. To determine whether the large plaque phenotype was present prior to the oral inoculation of mice, we performed plaque assays with our CVB3/ATCC and CVB3/IC

inoculum. Consistent with our in vivo data, the CVB3/ATCC inoculum plaque assay resulted in enhanced plaque size compared to CVB3/IC. Not only did the large plaque phenotype persist when the oral inoculation amount was lowered to $2x10^7$, the plaque assays performed following viral extraction of infected tissues also showed the CVB3/ATCC variant resulting in larger plaques than CVB3/IC.

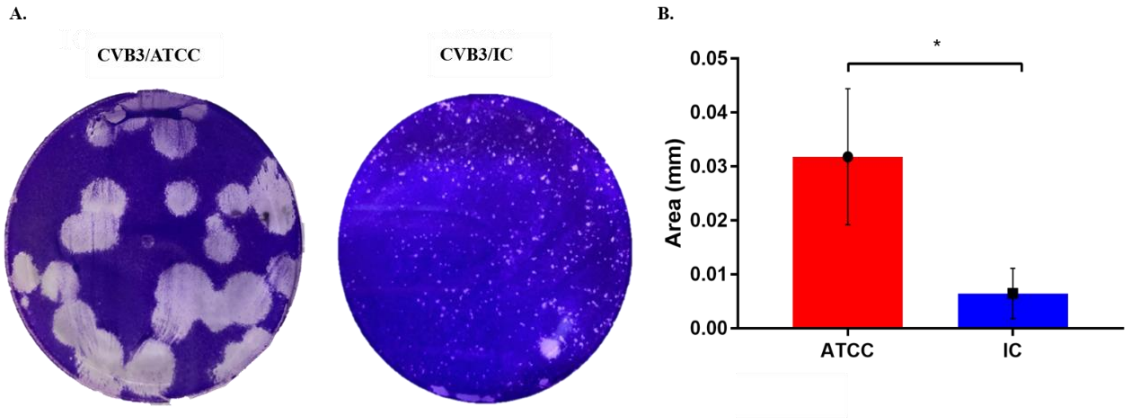

Figure 8: CVB3/ATCC displays a large plaque phenotype. (A) HeLa cell monolayers were inoculated with CVB3/ATCC or CVB3/IC virus extracted from feces collected 72 hpi and covered with an agar overlay for 48 hours. Following removal of agar plugs, cells were stained with 2% crystal violet solution. (B) Plaque diameter was quantified using ImageJ software ($p<0.0001$).

4.4 CVB3/ATCC exhibits enhanced cell attachment in HeLa cells

Our cell culture data indicated a difference in replication efficiency between the CVB3-Nancy variants CVB3/ATCC and CVB3/IC. Previously, CVB3 variants have displayed an altered binding phenotype as a result of mutations mapped to the capsid protein coding regions[86, 90, 99]. To investigate attachment efficiency in our CVB3 variants, HeLa cells were infected with either CVB3/ATCC or CVB3/IC at a MOI of 10 and incubated for 30 minutes at 4°C to allow virus to bind to but not enter cells. Following repeated washing with ice cold PBS, RNA was extracted and subject to real-time PCR targeting the VP1 capsid gene. We found that HeLa cells infected with

CVB3/ATCC had increased viral genome copies associated with the cell compared with cells infected with CVB3/IC (Figure 9). These data suggest that CVB3/ATCC may confer enhanced cell attachment in HeLa cells.

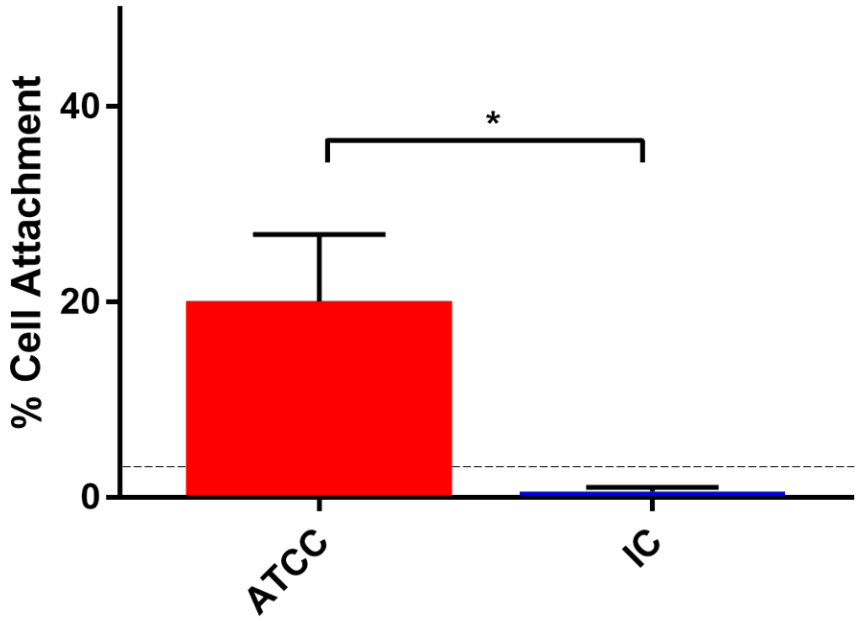

Figure 9: CVB3/ATCC exhibits increased in vitro cell attachment. HeLa or CHO cell monolayers were infected with an MOI of 10 of either CVB3/ATCC or CVB3/IC. Cell attachment was quantified via RT-PCR targeting viral VP1

Next, we performed immunohistochemical analysis to assess viral entry and translation. Following a 30-minute incubation at 37º C with CVB3/ATCC or CVB3/IC, HeLa cells were collected at 0, 2, 4, and 5 hpi and subject to western blot analysis. HeLa cells infected with CVB3/ATCC exhibited increased VP1 expression indicating increased viral translation (Figure 10).

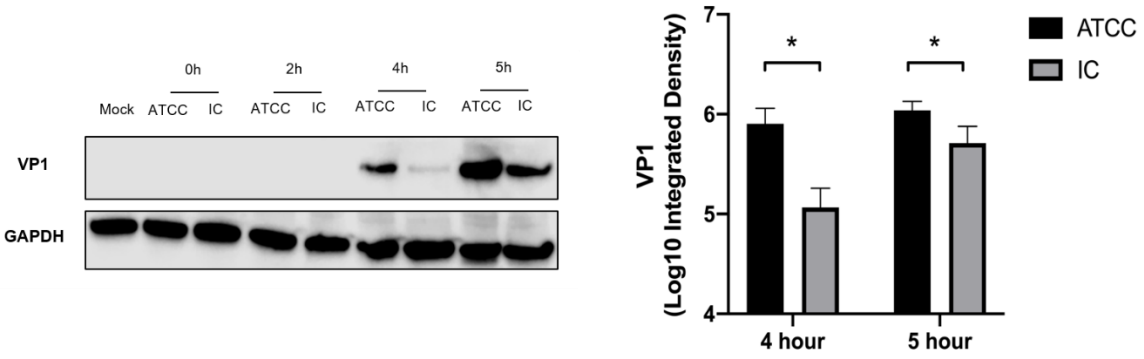

Figure 10: CVB3/ATCC exhibits increased viral translation. HeLa cells were incubation at 37º C for 30 minutes with CVB3/ATCC or CVB3/IC. HeLa cells were collected at 0, 2, 4, and 5 hpi and subject to western blot analysis. (A) VP1 expression in HeLa cell following CVB3 infection. (B) Quantification of VP1 expression at 4 and 5 hpi.

4.5 CVB3/ATCC infection results in increased CPE in cell culture

Our data indicate mutations in the CVB3/IC genome confer reduced viral fitness in cell culture. When compared to CVB3/IC, CVB3/ATCC exhibited enhanced growth and cell attachment therefore we next monitored CPE in HeLa and HCT-116 cells infected with either strain at a MOI of 10. As expected, both cell lines showed increased CPE when infected with CVB3/ATCC (Figure 11). Additionally, both Trypan blue and MTT assays revealed earlier onset of CPE in CVB3/ATCC infected cells with visible CPE at 16 hpi. These results further suggest the differences in genome sequence confer increased fitness in CVB3/ATCC.

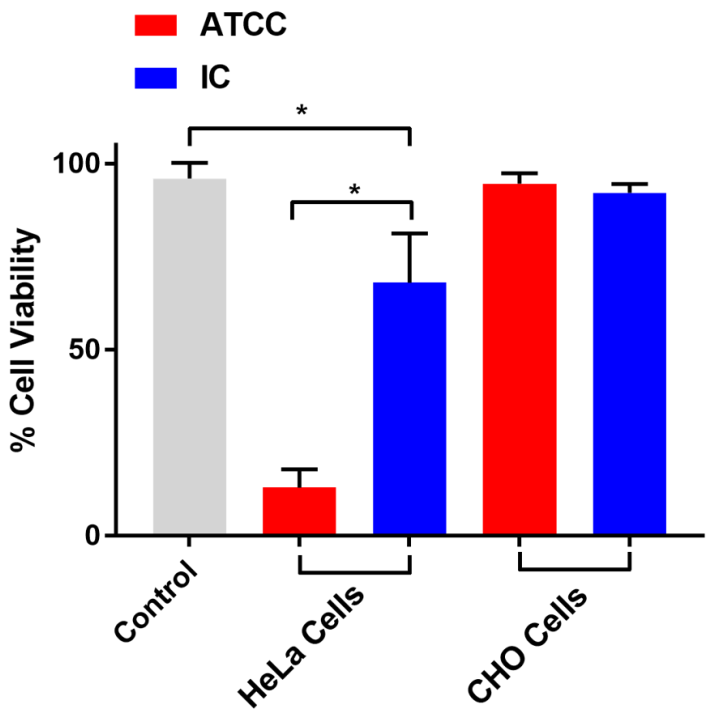

Figure 11: Trypan blue in vitro cell viability. HeLa or CHO cell monolayers were infected with an MOI of 10 of either CVB3/ATCC or CVB3/IC. Cell viability was assessed with Trypan blue at 48 hpi as CPE became apparent in HeLa cells.

4.6 CVB3/ATCC displays enhanced viral shedding and pathogenesis

We have established altered in vitro phenotypes resulting from differences in genome sequence between two CVB3-Nancy variants. To investigate whether these phenotypic differences translated to in vivo changes we sought to monitor viral shedding of CVB3 in the gastrointestinal tract. We orally inoculated immunodeficient C57BL/6 IFNAR knockout (IFNAR-/-) mice with $2x10^7$ PFU CVB3/ATCC or CVB3/IC. Fecal samples from infected mice were collected at 24, 48, and 72 hpi, and virus titers were determined by a plaque assay in HeLa cells. Feces collected at each time point were found to contain significantly higher viral titers in mice orally inoculated with CVB3/ATCC (Figure 12).

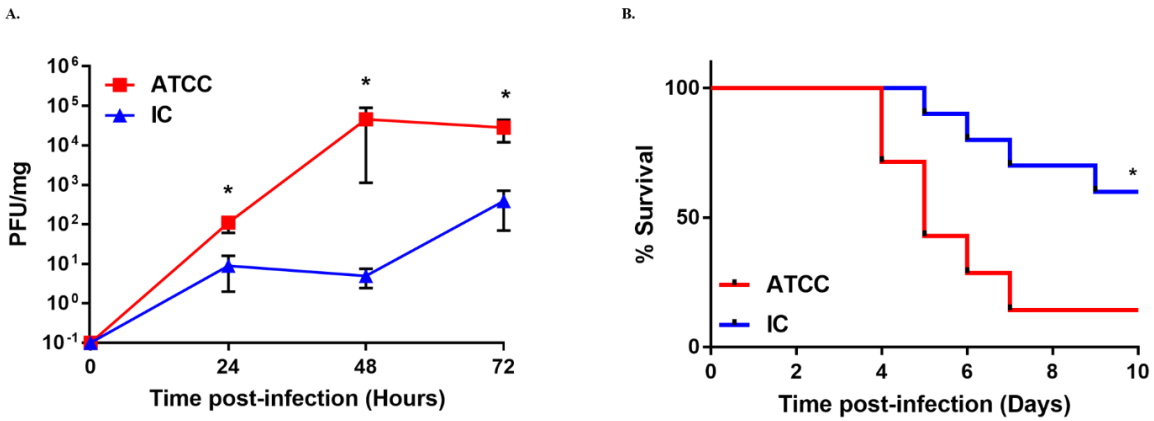

Figure 12: CVB3/ATCC results in enhanced viral shedding and decreased survival. IFNAR−/− mice orally inoculated with 2×107 PFU of CVB3/ATCC or CVB3/IC (A) Viral shedding assessed after collecting fecal samples at 0, 24, 48, and 72 hpi (n = 23 $p < 0.05$). (B) Survival measured following oral inoculation, critically ill mice were euthanized (n=7 $p < 0.05$). All data are means ± standard errors of the means (Mann-Whitney test).

To investigate the virulence of CVB3/ATCC strain versus CVB3/IC, we monitored the survival of mice following infection via oral inoculation of $2x10^7$ PFU. We found that survival following oral inoculation of CVB3/ATCC fell below 25%, whereas mice inoculated with CVB3/IC strain succumbed to infection at a much lower rate. Furthermore, IFNAR-/- mice infected CVB3/ATCC succumbed to infection sooner, on average succumbing to infection four days post infection whereas CVB3/IC infected mice began dying a full day later, on average. In summary, CVB3/ATCC exhibited enhanced viral fecal shedding, increased dissemination efficiency and was more pathogenic than CVB3/IC in IFNAR-/- mice (Figure 12).

4.7 CVB3/ATCC displays enhanced dissemination and increased hepatic damage

To discern cause of death in CVB3-infected IFNAR-/- mice and extrapolate the basis of increased pathogenicity observed in CVB3/ATCC infected mice, we examined various organ pathology. Upon euthanasia the heart, liver, kidneys, spleen, intestine and blood from IFNAR-/- mice orally inoculated with $2x10^7$ PFU CVB3/ATCC or CVB3/IC

were aseptically removed and flash frozen in liquid nitrogen or preserved in 10% neutral buffered formalin. Plaque assay revealed substantially higher viral titers in all organs removed from CVB3/ATCC mice when compared to CVB3/IC and control mice. Next, we examined viral titers in various tissues from orally inoculated IFNAR-/- mice at 72 hpi. Immediately following euthanasia 72 hpi, the heart, liver, kidney, spleen, intestine and serum were aseptically removed from each mouse. Tissues were homogenized and viral RNA extracted with TRIzol reagent. We found CVB3/ATCC titers were significantly higher than CVB3/IC titers in all IFNAR-/- mouse tissues examined. In contrast, preliminary experiments reveal lower viral titers in CVB3/IC infected mouse tissues, indicating increased dissemination to organ tissues distant from the gut in IFNAR-/- mice inoculated with CVB3/ATCC (data not shown).

In particular, the livers extracted from CVB3/ATCC infected mice revealed significantly higher viral titers than CVB3/IC infected mice. Previous work conducted by Wessely et al. as well as Pfeiffer et al. demonstrated that CVB3-infected IFNAR-/- mice develop liver pathology[89, 99]. To further examine the extent the livers were damaged, we measured the levels of alanine aminotransferase (ALT), a marker of liver damage, in serum. ALT levels remained low in control and CVB3/IC infected mice at 72 hpi. In contrast, ALT levels were significantly elevated at 72 hpi in mice infected with CVB3/ATCC (Figure 13).

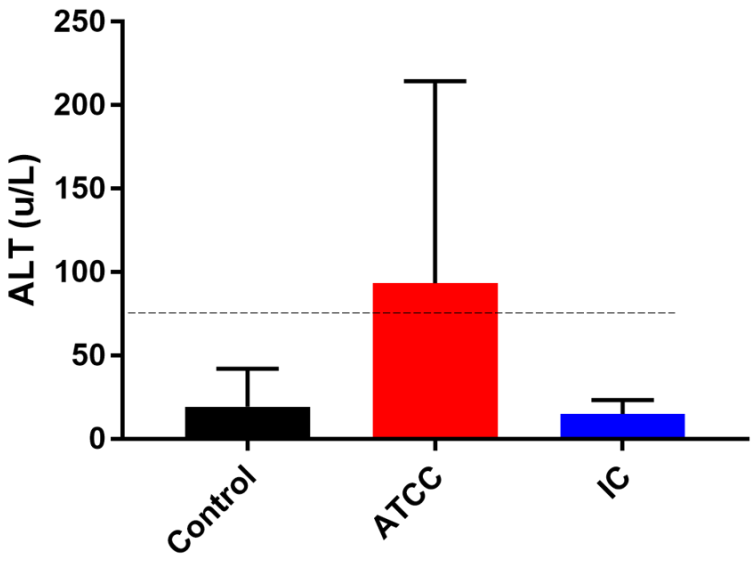

Figure 13: Serum ALT levels following CVB3 infection. ALT levels measured in serum collected at 72 hpi from IFNAR−/− mice orally inoculated with 2×10^7 PFU of CVB3/ATCC or CVB3/IC.

To investigate direct liver damage caused by CVB3 infection, we performed histological analysis of liver tissue harvested from mice at 72 hpi and found that mice infected with both the ATCC strain and IC strain displayed liver damage as measured by histology when compared with uninfected mice. Histological examination revealed visible hepatic cell necrosis and inflammation (Figure 14). As previously reported by Wessely and Pfeiffer, our data suggest that CVB3-infected IFNAR-/- mice develop liver damage and furthermore, CVB3/ATCC conferred enhanced liver damage [99, 106].

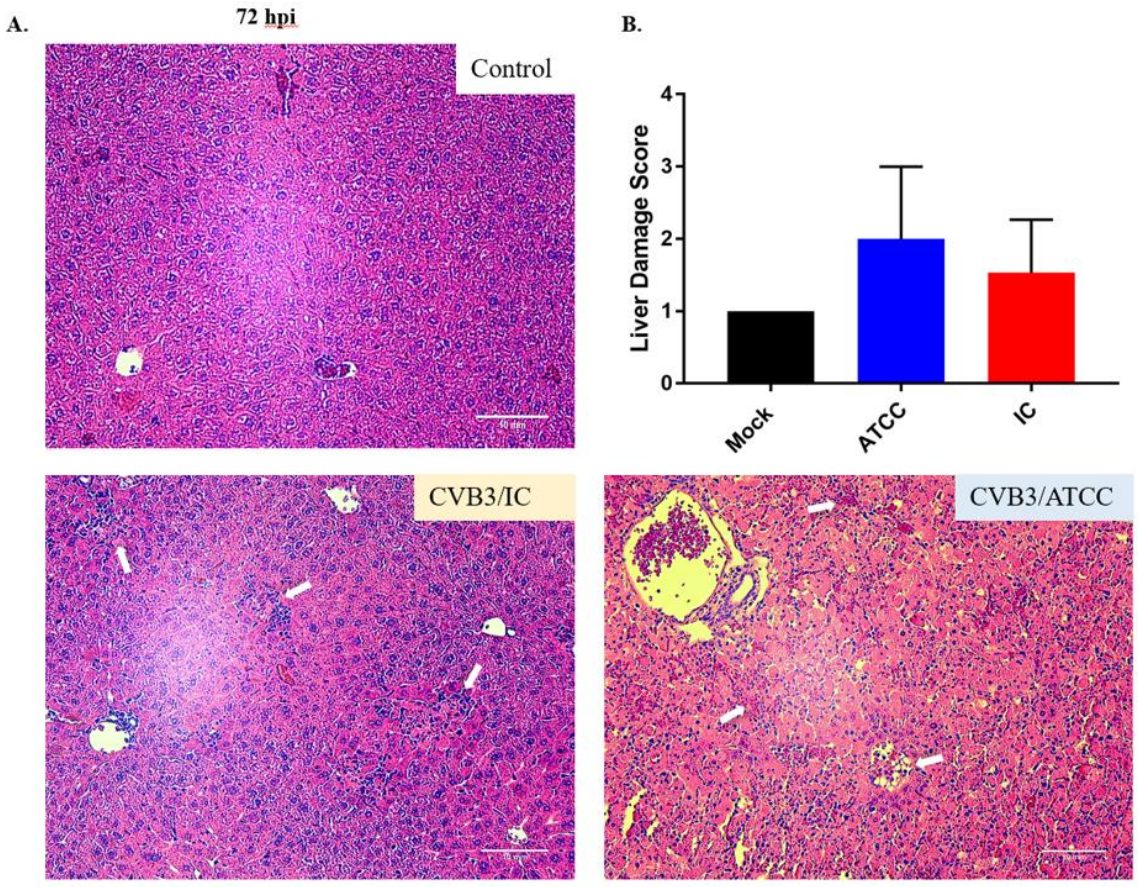

Figure 14: Histopathology of liver damage caused by CVB3 variants. Mice were inoculated with $2x10^7$ PFU CVB3/IC or CVB3/ATCC at 8-10 weeks of age. Livers were removed and harvested at 72 hpi and immediately preserved in 10% NBF. (A) Tissue samples were stained with H&E and given a pathology score (B) Evaluation of hepatic pathology by pathological scoring. 100x magnification.

CHAPTER FIVE

5. Discussion

Coxsackievirus B3 (CVB3) is an enteric virus that has been implicated in widespread human disease. Although CVB3 infection often presents with mild symptoms in humans, it has the potential to cause substantial sequelae in a small portion of the population. Previously, it has been shown that mutations found in certain areas of the CVB3 genome confer varying levels of pathogenicity and virulence[49, 53, 77, 82, 85, 87, 89, 92, 93, 95, 96, 100, 107, 108]. These observed disparities in viral fitness can been attributed to single polymorphisms mapped to the viral genome, however, research is still needed to understand the mechanism by which these discrepancies confer enhanced viral fitness.

Due to the lack of proofreading ability and genomic editing during RNA replication, the viral genome of RNA viruses is considerably error prone. Consequently, RNA viruses such as CVB3 accumulate mutations during each replicative cycle. The majority of the errors in the viral genome prove inconsequential, however, mutations found in certain areas of the genome such as structural coding sequences can exert a profound effect on viral fitness. Despite possible drawbacks arising from a high mutation rate, the highly diverse populations that result in few replication cycles are considered the basis for their rapid adaptation to new environments [109-111]. Advantageous mutations may result in new variants capable of escaping immune responses, resisting antiviral approaches, altering tissue tropism or crossing species barriers [111].

In this study we examined the attenuating effects of mutations found in the P1 region of CVB3/IC. While conducting in vivo experiments with CVB3-Nancy obtained

from two different sources, marked differences in viral virulence were observed. Using our novel oral inoculation method, C57BL/6 PVR and C57BL/6 PVR IFNAR−/− mice were inoculated with 2×10^7 PFU of CVB3-Nancy obtained from the American Type Culture Collection (ATCC) or from an infectious clone. Following infection, mice inoculated with CVB3/IC displayed attenuated pathogenesis. Several labs prior research have observed in vivo effects such as increased cardio-virulence [107] and increased hepatic damage [99] arising from genetic mutations found in the viral genome [67, 86, 106].

Amino acid differences among fully sequenced CVB3-Nancy variants															
Protein Region	**a.a. position**	**ATCC**	**IC**	**Coxsackievirus B3-Nancy (M)**	**P**	**PD**	**o**	**20 Klump/Tracy**	**28/HA**	**GA**	**31-1-93**	**RD**	**MKP**	**AH30**	**H3**
VP1	80	E	**K**	E	**K**	**A**	E	**K**	E	E	E	E	E	E	E
	92	L	L	**I**	L	**I**	L	L	L	**V**	L	**I**	L	**V**	**I**
VP2	13	**A**	**A**	V	**A**	V	**A**	V	**A**	V	V	V	**A**	V	V
	166	K	**Q**	K	K	K	K	K	K	K	K	K	**E**	K	K
VP3	63	N	**D**	N	N	N	N	N	N	N	N	N	N	N	N
	155	**I**	**I**	V	V	V	V	V	V	V	V	V	V	V	V
	178	Y	**F**	Y	Y	Y	Y	**F**	Y	Y	Y	Y	Y	Y	Y
VP4	16	**R**	**R**	G	G	G	G	**R**	G	G	G	G	G	G	G
5'UTR	nt 610	C	T	T	C	C	T	T	T	T	T	T	T	G	T
2A	92	R	G	R	R	R	R	R	R	K	R	R	R	K	R

Table 2: Amino acid polymorphisms distinguishing CVB3 Nancy variants. Comparing CVB3/ATCC and CVB3/IC with 11 fully sequenced CVB3 Nancy variants. Bold amino acid indicated mutations not seen in WT.

To study the molecular basis of the observed variations in pathogenesis, the complete viral genome of CVB3/ATCC and CVB3/IC were sequenced. The results reveal a high amino acid homology among the CVB3 strains found in (Table 1). In comparing the genome of CVB3/IC to that of the published amino acid sequence for the wild type CVB3-Nancy M (M16572) and CVB3/ATCC genome, we identified several amino acid substitutions in the P1 structural coding region of the CVB3/IC genome (Table 2). Further, when compared to several CVB3 variants, sequence alignment revealed a

number of mutations in the CVB3/IC genome located in areas of the capsid shown to be integral in viral cell attachment. Mutations identified at VP1 residues E80K, I92L, and V180I, Vp2 residues I108V, N138D, and T151S, as well as VP3 residues N63D, Y178F, and E234Q were investigated further based on location within the capsid and implications on virus-receptor binding (Table 3).

Using the MISSENSE computer software program, mutations were virtually introduced into the CVB3 genome at these locations, with VP1 I92L being the only mutation conferring structural capsid damage (Table 3). Carson et al., found that a single substitution of valine VP1 residue 92 was individually capable of stabilizing the virus the normally unstable CVB3/28 laboratory propagated virus. Further, Carson et al. found leucine at VP1 residue 92 in only 4% of CVB3 sequences screened, most of which relating to CVB3/Nancy [85]. Furthermore, residue 92 lies in the hydrophobic pocket of VP1 where the stabilizing lipid, the pocket factor, and stabilizing antiviral compounds are bound [96, 98, 105]. Leucine at VP1 residue 92 has been shown to associate with CVB3 resistance to pleconaril [98]. When isoleucine is substituted with leucine VP1 residue 92 in the CVB3 capsid protein structure obtained from the RCSB Protein Data Bank (PDB) the resulting structure conflicts with the leucine sidechain and the critical pocket factor. Considering, as Reisdorph et al. concluded, the importance of the pocket-binding molecules and of the pocket in the conformational capsid breathing, VP1 residue 92 would appear to be a key determinant of virus stability [112]. As leucine at VP1 residue 92 has been identified predominantly in CVB3 laboratory strains (related to Nancy), as well as strains selected for resistance to antiviral drugs [113, 114] it is possible that a less stable virus is favored when selection works against more stable virus populations. Taken

together it should not be surprising that the CVB3/IC mutant possesses the rare leucine mutation at VP1 residue 92 as the strain has been continually passaged in HeLa cells. Finally, Carson et al., found that the less stable CVB3/28 uncoated more rapidly suggesting that laboratory propagation of these viruses in receptor rich cell cultures can select for the less stable variants in the quasi-species because they can uncoat more rapidly and commandeer the replication resources of the host cells [85, 96].

Region	a.a.	CVB3 Nancy	ATCC	IC	Structural effect
VP2	13	V	A	A	The substitution leads to the expansion of cavity volume by 12.312 Å^3
VP3	63	N	N	**D**	The wild-type residue ASN is exposed uncharged with RSA 80.8% and the mutant residue ASP is exposed negative-charged with RSA 74.8%
	178	Y	Y	**F**	No effect
VP1	80	E	E	**K**	Wild-type salt bridge is detected between OE2 atom of GLU 80 and NZ atom of LYS 85 (distance: 4.453 Å) is disrupted by the substitution this bond. The wild-type residue GLU is exposed negative-charged with RSA 23.7% and the mutant residue LYS is exposed positive-charged with RSA 35.6%.
	92	I	L	L	The substitution leads to the contraction of cavity volume by 93.744 Å^3
	180	V	I	I	The substitution leads to the contraction of cavity volume by 32.4 Å^3

Table 3: Theoretical structural effects of CVB3 mutations. Comparison of single polymorphisms between CVB3/ATCC and CVB3/IC. Using the virtual mutagenesis software MISSENSE, individual mutations found in CVB3/IC were introduced into the CVB3 Nancy genome and possible effects outlined.

In addition to the substitution of isoleucine with leucine at VP1 residue 92, we observed additional VP1 substitutions, including E80K and V180I. In contrast, Carson et al., found that the single capsid mutation from glutamate to lysine at VP1 residue 80 was present in the more stable CVB3/28 strain. Whereas glutamate at VP1 residue 80

dominates CVB3 sequences, lysine dominates this position in CVB5 and CVB6, suggesting that the residue in this position may be favored by pairing with other differences between serotypes [85, 90, 96, 98]. It is likely that glutamate may participate in ionic interaction with the three nearby positively charged side chains, while lysine will contribute to a positive charge cluster that may increase the capsid interaction with anionic secondary ligands. Although the VP1 mutation I92L observed in CVB3/IC may be implicated in a less stable virus, the mutation E80K has been associated with the more stable virus. This disagreement may arise from individual selection pressures, duration of adaption to cell culture, or the weight of the mutational effects. CVB3/IC replication in HeLa cells as well as in vivo are significantly attenuated thereby implying a less stable virion.

The most interesting mutations observed in CVB3/IC are those located in the VP2 and VP3 regions. These mutations include N138D found in VP2 and the VP3 mutations N63D and E234Q. Notably, N138D lies in the EF loop a large and highly variable surface loop of VP2 proteins of all enteroviruses, referred to as the puff region. The puff region is known to be a major neutralization site in both polioviruses and rhinoviruses and is also variable between intertypic and intratypic variants of group B coxsackieviruses [86]. Additionally, studies conducted on clinical isolates of CVB3 revealed several mutations in the puff region were implicated in the development of myocarditis as opposed to non-myocarditis strains [89]. Previously, Pan et al., examined the effects of the VP2-138D mutation and found it to be important for CVB3 interaction with DAF. In fact, Pan et al., found that both mutations found in our CVB3/IC mutant, VP3-234Q and VP2-138D, were required for virus attachment to DAF [92, 115]. These

results may help to explain disparities observed between CVB3/IC and CVB3/ATCC in CAR-rich HeLa cells where CAR is readily accessible versus HCT-116 cells. Wild type CVB3-Nancy replicates in HeLa cells more efficiently than CVB3/IC, however, in HCT-116 cells CVB3/IC may exhibit enhanced replication efficiency most likely due to the availability of DAF among the cell types. Indeed, Borderia et al. demonstrated adaptation occurring in response to a differential expression of the virus receptors in the new cellular environment. Borderia et al. found in HeLa cells, where both CAR and DAF are highly and ubiquitously expressed on the surface, adaptive mutations in the VP regions mapped to both CAR and DAF footprints, although it was unclear whether the CAR-specific mutations observed in HeLa cells increased interactions with CAR, or conversely, decreased interactions to facilitate the appearance of other mutations related to the DAF footprint [111, 116].

Recently, Wang and Pfeiffer described the CVB3-Nancy VP3 N63Y mutation, finding that the single mutation conferred a large plaque phenotype, enhanced hepatic damage, as well as diminished growth in cell culture. Additionally, Bordería et al. demonstrated viral passage in A549 human lung cells resulted in polymorphisms at position 63 of VP3, including N63Y, N63D, and N63H [111]. Notably, VP3 residues 58-69 form the knob which is the major surface protrusion of VP3 [105]. Taken together, these results indicate the highly conserved N63 may play a sizable role in the altered phenotype we have observed in our CVB3/IC mutant. Furthermore, whereas the N63Y mutation described by Wang and Pfeiffer resulted in a large plaque phenotype, the N63D mutant results in a small plaque phenotype. In cell culture, the N63Y mutation resulted in

a growth defect in a variety of cell lines and N63Y also exhibited a significant reduction in cell attachment.

In agreement with Wang and Pfeiffer we found the N63D mutant to display decreased cell attachment. In vivo studies performed by Wang and Pfeiffer, however, found enhanced liver pathology in mice infected with N63Y mutant CVB3, as well as increased replication and pathogenesis when compared with wild type CVB3. In contrast, the N63D mutant results in a significant attenuation in viral replication and pathogenesis in both immunocompetent and IFNAR-/- mice. These results suggest the single mutation found at VP3 N63 can exert significant effects on viral cell attachment and replication in vitro as well as in vivo pathogenesis in mice.

In addition to the main Coxsackie-adenovirus receptor, CVB3 exhibits the ability to bind heparin sulfate or other glycosaminoglycans GAGs thereby enhancing cell attachment [117]. Interestingly, GAGs most commonly interact with viral particles via positively charged amino acids such as lysine or arginine [99]. Whereas the N63Y mutant CVB3 results in a change from a positively charged asparagine to an uncharged tyrosine thereby disrupting potential GAG binding the mutation we have observed N63D results in a change in charge to the negatively charged aspartic acid. It is likely therefore, that the opposite charge resulting from the N63D mutation may lead to a diminished ability of the virus to bind to HS or GAG resulting in decreased cell attachment both in vivo and in vitro.

The aggregation of observed mutations identified in our CVB3/IC mutant seem to encompass conflicting phenotypes. Whereas the VP1 mutation E80K has been associated with increased viral stability, I92L is implicated in viral instability. Mutations observed in

the VP2 and VP3 regions, however, are associated with increased DAF binding. The particular combination of mutations found in CVB3/IC, resulting in attenuated viral replication and pathogenesis both in vitro and in vivo. The results indicate the significant contribution of several minority variants to the overall fitness of the virus population over time.

In conclusion, our data indicate that mutations found within the CVB3 genome, especially those found in the 5' UTR as well as the VP regions, exert considerable influence on viral fitness. As our experiments and those performed in other labs demonstrate, single amino acid substitutions found at VP1 E80K and VP3 N63D play a role in viral stability, virus-host-cell-receptor interaction, and in vivo pathogenesis. Further research should focus on confirming these findings and identifying molecular mechanisms via viral mutagenesis. Identifying the molecular mechanism involved in how these mutations contribute to the pathogenesis of disease in humans will lead to better strategies for refining prognosis, treatment, and vaccination development.

REFERENCES

1. Wu, Q., et al., *Prevalence of enteroviruses in healthy populations and excretion of pathogens in patients with hand, foot, and mouth disease in a highly endemic area of southwest China.* PLoS One, 2017. **12**(7): p. e0181234.
2. Strikas, R.A., L.J. Anderson, and R.A. Parker, *Temporal and geographic patterns of isolates of nonpolio enterovirus in the United States, 1970-1983.* J Infect Dis, 1986. **153**(2): p. 346-51.
3. Fendrick, A.M., et al., *The economic burden of non-influenza-related viral respiratory tract infection in the United States.* Arch Intern Med, 2003. **163**(4): p. 487-94.
4. Solomon, T., et al., *Virology, epidemiology, pathogenesis, and control of enterovirus 71.* Lancet Infect Dis, 2010. **10**(11): p. 778-90.
5. Pons-Salort, M., E.P. Parker, and N.C. Grassly, *The epidemiology of non-polio enteroviruses: recent advances and outstanding questions.* Curr Opin Infect Dis, 2015. **28**(5): p. 479-87.
6. Khatami, A., et al., *Sepsis-like disease in infants due to human parechovirus type 3 during an outbreak in Australia.* Clin Infect Dis, 2015. **60**(2): p. 228-36.
7. Chang, P.C., S.C. Chen, and K.T. Chen, *The Current Status of the Disease Caused by Enterovirus 71 Infections: Epidemiology, Pathogenesis, Molecular Epidemiology, and Vaccine Development.* Int J Environ Res Public Health, 2016. **13**(9).
8. Harvala, H., et al., *Recommendations for enterovirus diagnostics and characterisation within and beyond Europe.* J Clin Virol, 2018. **101**: p. 11-17.
9. Wolthers, K.C., et al., *Progress in human picornavirus research: New findings from the AIROPico consortium.* Antiviral Res, 2019. **161**: p. 100-107.
10. Baggen, J., et al., *The life cycle of non-polio enteroviruses and how to target it.* Nat Rev Microbiol, 2018. **16**(6): p. 368-381.
11. Heikkila, O., M. Kainulainen, and P. Susi, *A combined method for rescue of modified enteroviruses by mutagenic primers, long PCR and T7 RNA polymerase-driven in vivo transcription.* J Virol Methods, 2011. **171**(1): p. 129-33.
12. Merilahti, P., et al., *Endocytosis of integrin-binding human picornaviruses.* Adv Virol, 2012. **2012**: p. 547530.
13. Holland, J.J., et al., *Enteroviral ribonucleic acid. II. Biological, physical, and chemical studies.* J Exp Med, 1960. **112**: p. 841-64.
14. Hafenstein, S., *Structural biology: A picornavirus unlike the others.* Nat Microbiol, 2016. **1**(11): p. 16217.
15. Sin, J., et al., *Recent progress in understanding coxsackievirus replication, dissemination, and pathogenesis.* Virology, 2015. **484**: p. 288-304.
16. Rossmann, M.G., et al., *Structure of a human common cold virus and functional relationship to other picornaviruses.* Nature, 1985. **317**(6033): p. 145-53.
17. Hogle, J.M., M. Chow, and D.J. Filman, *Three-dimensional structure of poliovirus at 2.9 A resolution.* Science, 1985. **229**(4720): p. 1358-65.
18. Ren, J., et al., *Structures of Coxsackievirus A16 Capsids with Native Antigenicity: Implications for Particle Expansion, Receptor Binding, and Immunogenicity.* J Virol, 2015. **89**(20): p. 10500-11.

19. Shakeel, S., et al., *Structural Basis of Human Parechovirus Neutralization by Human Monoclonal Antibodies.* J Virol, 2015. **89**(18): p. 9571-80.
20. Emini, E.A., et al., *Antigenic conservation and divergence between the viral-specific proteins of poliovirus type 1 and various picornaviruses.* Virology, 1985. **140**(1): p. 13-20.
21. Norder, H., et al., *Picornavirus non-structural proteins as targets for new anti-virals with broad activity.* Antiviral Res, 2011. **89**(3): p. 204-18.
22. Rotbart, H.A., *Treatment of picornavirus infections.* Antiviral Res, 2002. **53**(2): p. 83-98.
23. Dalldorf, G. and G.M. Sickles, *An Unidentified, Filtrable Agent Isolated From the Feces of Children With Paralysis.* Science, 1948. **108**(2794): p. 61-2.
24. Garmaroudi, F.S., et al., *Coxsackievirus B3 replication and pathogenesis.* Future Microbiol, 2015. **10**(4): p. 629-53.
25. Melnick, J.L., E.W. Shaw, and E.C. Curnen, *A virus isolated from patients diagnosed as non-paralytic poliomyelitis or aseptic meningitis.* Proc Soc Exp Biol Med, 1949. **71**(3): p. 344-9.
26. Melnick, J.L., *Portraits of viruses: the picornaviruses.* Intervirology, 1983. **20**(2-3): p. 61-100.
27. Centers for Disease, C. and Prevention, *Nonpolio enterovirus and human parechovirus surveillance --- United States, 2006-2008.* MMWR Morb Mortal Wkly Rep, 2010. **59**(48): p. 1577-80.
28. Romero, J.R., *Pediatric group B coxsackievirus infections.* Curr Top Microbiol Immunol, 2008. **323**: p. 223-39.
29. Kosrirukvongs, P., et al., *Acute hemorrhagic conjunctivitis outbreak in Thailand, 1992.* Southeast Asian J Trop Med Public Health, 1996. **27**(2): p. 244-9.
30. He, S.J., et al., *Characterization of enterovirus 71 and coxsackievirus A16 isolated in hand, foot, and mouth disease patients in Guangdong, 2010.* Int J Infect Dis, 2013. **17**(11): p. e1025-30.
31. Andreoletti, L., et al., *Viral causes of human myocarditis.* Arch Cardiovasc Dis, 2009. **102**(6-7): p. 559-68.
32. David, P., et al., *MRI of acute disseminated encephalomyelitis after coxsackie B infection.* J Neuroradiol, 1993. **20**(4): p. 258-65.
33. Ornoy, A. and A. Tenenbaum, *Pregnancy outcome following infections by coxsackie, echo, measles, mumps, hepatitis, polio and encephalitis viruses.* Reprod Toxicol, 2006. **21**(4): p. 446-57.
34. Euscher, E., et al., *Coxsackie virus infection of the placenta associated with neurodevelopmental delays in the newborn.* Obstet Gynecol, 2001. **98**(6): p. 1019-26.
35. Rhoades, R.E., et al., *Enterovirus infections of the central nervous system.* Virology, 2011. **411**(2): p. 288-305.
36. Robinson, C.M., Y. Wang, and J.K. Pfeiffer, *Sex-Dependent Intestinal Replication of an Enteric Virus.* J Virol, 2017. **91**(7).
37. Huber, S.A., C.J. Gauntt, and P. Sakkinen, *Enteroviruses and myocarditis: viral pathogenesis through replication, cytokine induction, and immunopathogenicity.* Adv Virus Res, 1998. **51**: p. 35-80.

38. Rohll, J.B., et al., *The 5'-untranslated regions of picornavirus RNAs contain independent functional domains essential for RNA replication and translation.* J Virol, 1994. **68**(7): p. 4384-91.
39. Flanegan, J.B., et al., *Covalent linkage of a protein to a defined nucleotide sequence at the 5'-terminus of virion and replicative intermediate RNAs of poliovirus.* Proc Natl Acad Sci U S A, 1977. **74**(3): p. 961-5.
40. Selinka, H.C., et al., *Virus-receptor interactions of coxsackie B viruses and their putative influence on cardiotropism.* Med Microbiol Immunol, 2004. **193**(2-3): p. 127-31.
41. Selinka, H.C., et al., *Comparative analysis of two coxsackievirus B3 strains: putative influence of virus-receptor interactions on pathogenesis.* J Med Virol, 2002. **67**(2): p. 224-33.
42. Zautner, A.E., et al., *Heparan sulfates and coxsackievirus-adenovirus receptor: each one mediates coxsackievirus B3 PD infection.* J Virol, 2003. **77**(18): p. 10071-7.
43. Ehrenfeld, E., *Poliovirus-induced inhibition of host-cell protein synthesis.* Cell, 1982. **28**(3): p. 435-6.
44. Badorff, C., et al., *Enteroviral protease 2A directly cleaves dystrophin and is inhibited by a dystrophin-based substrate analogue.* J Biol Chem, 2000. **275**(15): p. 11191-7.
45. Leveque, N., et al., *Functional Consequences of RNA 5'-Terminal Deletions on Coxsackievirus B3 RNA Replication and Ribonucleoprotein Complex Formation.* J Virol, 2017. **91**(16).
46. Andino, R., G.E. Rieckhof, and D. Baltimore, *A functional ribonucleoprotein complex forms around the 5' end of poliovirus RNA.* Cell, 1990. **63**(2): p. 369-80.
47. Hunziker, I.P., C.T. Cornell, and J.L. Whitton, *Deletions within the 5'UTR of coxsackievirus B3: consequences for virus translation and replication.* Virology, 2007. **360**(1): p. 120-8.
48. Cunningham, K.A., N.M. Chapman, and S.D. Carson, *Caspase-3 activation and ERK phosphorylation during CVB3 infection of cells: influence of the coxsackievirus and adenovirus receptor and engineered variants.* Virus Res, 2003. **92**(2): p. 179-86.
49. McManus, B.M., et al., *Genetic determinants of coxsackievirus B3 pathogenesis.* Ann N Y Acad Sci, 2002. **975**: p. 169-79.
50. Opavsky, M.A., et al., *Enhanced ERK-1/2 activation in mice susceptible to coxsackievirus-induced myocarditis.* J Clin Invest, 2002. **109**(12): p. 1561-9.
51. Chang, L. and M. Karin, *Mammalian MAP kinase signalling cascades.* Nature, 2001. **410**(6824): p. 37-40.
52. Van Houten, N. and S.A. Huber, *Genetics of Coxsackie B3 (CVB3) myocarditis.* Eur Heart J, 1991. **12 Suppl D**: p. 108-12.
53. Prusa, J., et al., *Major alteration in coxsackievirus B3 genomic RNA structure distinguishes a virulent strain from an avirulent strain.* Nucleic Acids Res, 2014. **42**(15): p. 10112-21.
54. Klump, W.M., et al., *Complete nucleotide sequence of infectious Coxsackievirus B3 cDNA: two initial 5' uridine residues are regained during plus-strand RNA synthesis.* J Virol, 1990. **64**(4): p. 1573-83.

55. Lindberg, A.M., P.O. Stalhandske, and U. Pettersson, *Genome of coxsackievirus B3.* Virology, 1987. **156**(1): p. 50-63.
56. Couderc, T., et al., *Molecular characterization of mouse-virulent poliovirus type 1 Mahoney mutants: involvement of residues of polypeptides VP1 and VP2 located on the inner surface of the capsid protein shell.* J Virol, 1993. **67**(7): p. 3808-17.
57. Kandolf, R. and P.H. Hofschneider, *Molecular cloning of the genome of a cardiotropic Coxsackie B3 virus: full-length reverse-transcribed recombinant cDNA generates infectious virus in mammalian cells.* Proc Natl Acad Sci U S A, 1985. **82**(14): p. 4818-22.
58. M'Hadheb-Gharbi, M.B., K.M. Kean, and J. Gharbi, *Molecular analysis of the role of IRES stem-loop V in replicative capacities and translation efficiencies of Coxsackievirus B3 mutants.* Mol Biol Rep, 2009. **36**(2): p. 255-62.
59. Sharma, N., et al., *Functional role of the 5' terminal cloverleaf in Coxsackievirus RNA replication.* Virology, 2009. **393**(2): p. 238-49.
60. Murray, K.E., et al., *Replication of poliovirus RNA with complete internal ribosome entry site deletions.* J Virol, 2004. **78**(3): p. 1393-402.
61. Pelletier, J. and N. Sonenberg, *Internal initiation of translation of eukaryotic mRNA directed by a sequence derived from poliovirus RNA.* Nature, 1988. **334**(6180): p. 320-5.
62. Bhattacharyya, S., et al., *The structure and function of a cis-acting element located upstream of the IRES that influences Coxsackievirus B3 RNA translation.* Virology, 2008. **377**(2): p. 345-54.
63. Lee, C.K., et al., *Characterization of an infectious cDNA copy of the genome of a naturally occurring, avirulent coxsackievirus B3 clinical isolate.* J Gen Virol, 2005. **86**(Pt 1): p. 197-210.
64. Liu, Z., et al., *Structural and functional analysis of the 5' untranslated region of coxsackievirus B3 RNA: In vivo translational and infectivity studies of full-length mutants.* Virology, 1999. **265**(2): p. 206-17.
65. Svitkin, Y.V., et al., *Translation deficiency of the Sabin type 3 poliovirus genome: association with an attenuating mutation C472----U.* Virology, 1990. **175**(1): p. 103-9.
66. Evans, D.M., et al., *Increased neurovirulence associated with a single nucleotide change in a noncoding region of the Sabin type 3 poliovaccine genome.* Nature, 1985. **314**(6011): p. 548-50.
67. Tu, Z., et al., *The cardiovirulent phenotype of coxsackievirus B3 is determined at a single site in the genomic 5' nontranslated region.* J Virol, 1995. **69**(8): p. 4607-18.
68. Mahmud, B., C.M. Horn, and W.E. Tapprich, *Structure of the 5' Untranslated Region of Enteroviral Genomic RNA.* J Virol, 2019. **93**(23).
69. Bailey, J.M. and W.E. Tapprich, *Structure of the 5' nontranslated region of the coxsackievirus b3 genome: Chemical modification and comparative sequence analysis.* J Virol, 2007. **81**(2): p. 650-68.
70. Bradrick, S.S., et al., *A predicted secondary structural domain within the internal ribosome entry site of echovirus 12 mediates a cell-type-specific block to viral replication.* J Virol, 2001. **75**(14): p. 6472-81.

71. Dunn, J.J., et al., *The stem loop II within the 5' nontranslated region of clinical coxsackievirus B3 genomes determines cardiovirulence phenotype in a murine model.* J Infect Dis, 2003. **187**(10): p. 1552-61.
72. Jackson, R.J., et al., *Internal initiation of translation of picornavirus RNAs.* Mol Biol Rep, 1994. **19**(3): p. 147-59.
73. Ramos, R. and E. Martinez-Salas, *Long-range RNA interactions between structural domains of the aphthovirus internal ribosome entry site (IRES).* RNA, 1999. **5**(10): p. 1374-83.
74. Robertson, M.E., R.A. Seamons, and G.J. Belsham, *A selection system for functional internal ribosome entry site (IRES) elements: analysis of the requirement for a conserved GNRA tetraloop in the encephalomyocarditis virus IRES.* RNA, 1999. **5**(9): p. 1167-79.
75. M'Hadheb-Gharbi, M.B., et al., *Role of GNRA motif mutations within stem-loop V of internal ribosome entry segment in coxsackievirus B3 molecular attenuation.* J Mol Microbiol Biotechnol, 2008. **14**(4): p. 147-56.
76. Sabin, A.B., *Oral poliovirus vaccine. History of its development and prospects for eradication of poliomyelitis.* JAMA, 1965. **194**(8): p. 872-6.
77. M'Hadheb-Gharbi, M.B., et al., *The substitution U475 --> C with Sabin3-like mutation within the IRES attenuate Coxsackievirus B3 cardiovirulence.* Mol Biotechnol, 2007. **36**(1): p. 52-60.
78. Macadam, A.J., et al., *Correlation of RNA secondary structure and attenuation of Sabin vaccine strains of poliovirus in tissue culture.* Virology, 1992. **189**(2): p. 415-22.
79. Macadam, A.J., et al., *Genetic basis of attenuation of the Sabin type 2 vaccine strain of poliovirus in primates.* Virology, 1993. **192**(1): p. 18-26.
80. Ben M'hadheb-Gharbi, M., et al., *Effects of the Sabin-like mutations in domain V of the internal ribosome entry segment on translational efficiency of the Coxsackievirus B3.* Mol Genet Genomics, 2006. **276**(4): p. 402-12.
81. Souii, A., J. Gharbi, and M. Ben M'hadheb-Gharbi, *Impaired binding of standard initiation factors eIF3b, eIF4G and eIF4B to domain V of the live-attenuated coxsackievirus B3 Sabin3-like IRES--alternatives for 5'UTR-related cardiovirulence mechanisms.* Diagn Pathol, 2013. **8**: p. 161.
82. Ben M'hadheb, M., et al., *In vitro-reduced translation efficiency of coxsackievirus B3 Sabin3-like strain is correlated to impaired binding of cellular initiation factors to viral IRES RNA.* Curr Microbiol, 2015. **70**(5): p. 756-61.
83. Ramsingh, A.I. and D.N. Collins, *A point mutation in the VP4 coding sequence of coxsackievirus B4 influences virulence.* J Virol, 1995. **69**(11): p. 7278-81.
84. Organtini, L.J., et al., *Kinetic and structural analysis of coxsackievirus B3 receptor interactions and formation of the A-particle.* J Virol, 2014. **88**(10): p. 5755-65.
85. Carson, S.D., et al., *Three capsid amino acids notably influence coxsackie B3 virus stability.* J Gen Virol, 2016. **97**(1): p. 60-68.
86. Stadnick, E., et al., *Attenuating mutations in coxsackievirus B3 map to a conformational epitope that comprises the puff region of VP2 and the knob of VP3.* J Virol, 2004. **78**(24): p. 13987-4002.

87. Caggana, M., P. Chan, and A. Ramsingh, *Identification of a single amino acid residue in the capsid protein VP1 of coxsackievirus B4 that determines the virulent phenotype.* J Virol, 1993. **67**(8): p. 4797-803.
88. Zhang, H., et al., *A single amino acid substitution in the capsid protein VP1 of coxsackievirus B3 (CVB3) alters plaque phenotype in Vero cells but not cardiovirulence in a mouse model.* Arch Virol, 1995. **140**(5): p. 959-66.
89. Knowlton, K.U., et al., *A mutation in the puff region of VP2 attenuates the myocarditic phenotype of an infectious cDNA of the Woodruff variant of coxsackievirus B3.* J Virol, 1996. **70**(11): p. 7811-8.
90. Schmidtke, M., et al., *Attachment of coxsackievirus B3 variants to various cell lines: mapping of phenotypic differences to capsid protein VP1.* Virology, 2000. **275**(1): p. 77-88.
91. Cohen, C.J., et al., *The coxsackievirus and adenovirus receptor is a transmembrane component of the tight junction.* Proc Natl Acad Sci U S A, 2001. **98**(26): p. 15191-6.
92. Pan, J., et al., *Single amino acid changes in the virus capsid permit coxsackievirus B3 to bind decay-accelerating factor.* J Virol, 2011. **85**(14): p. 7436-43.
93. Bergelson, J.M., et al., *Clinical coxsackievirus B isolates differ from laboratory strains in their interaction with two cell surface receptors.* J Infect Dis, 1997. **175**(3): p. 697-700.
94. Shafren, D.R., et al., *Coxsackieviruses B1, B3, and B5 use decay accelerating factor as a receptor for cell attachment.* J Virol, 1995. **69**(6): p. 3873-7.
95. Reagan, K.J., B. Goldberg, and R.L. Crowell, *Altered receptor specificity of coxsackievirus B3 after growth in rhabdomyosarcoma cells.* J Virol, 1984. **49**(3): p. 635-40.
96. Carson, S.D., et al., *Variations of coxsackievirus B3 capsid primary structure, ligands, and stability are selected for in a coxsackievirus and adenovirus receptor-limited environment.* J Virol, 2011. **85**(7): p. 3306-14.
97. Paloheimo, O., et al., *Coxsackievirus B3-induced cellular protrusions: structural characteristics and functional competence.* J Virol, 2011. **85**(13): p. 6714-24.
98. Schmidtke, M., et al., *Susceptibility of coxsackievirus B3 laboratory strains and clinical isolates to the capsid function inhibitor pleconaril: antiviral studies with virus chimeras demonstrate the crucial role of amino acid 1092 in treatment.* J Antimicrob Chemother, 2005. **56**(4): p. 648-56.
99. Wang, Y. and J.K. Pfeiffer, *Emergence of a Large-Plaque Variant in Mice Infected with Coxsackievirus B3.* mBio, 2016. **7**(2): p. e00119.
100. Massilamany, C., et al., *Mutations in the 5' NTR and the Non-Structural Protein 3A of the Coxsackievirus B3 Selectively Attenuate Myocarditogenicity.* PLoS One, 2015. **10**(6): p. e0131052.
101. Sane, F., I. Moumna, and D. Hober, *Group B coxsackieviruses and autoimmunity: focus on Type 1 diabetes.* Expert Rev Clin Immunol, 2011. **7**(3): p. 357-66.
102. Chow, L.H., C.J. Gauntt, and B.M. McManus, *Differential effects of myocarditic variants of Coxsackievirus B3 in inbred mice. A pathologic characterization of heart tissue damage.* Lab Invest, 1991. **64**(1): p. 55-64.
103. Nei, M., *Phylogenetic analysis in molecular evolutionary genetics.* Annu Rev Genet, 1996. **30**: p. 371-403.

104. Kumar, S., et al., *MEGA X: Molecular Evolutionary Genetics Analysis across Computing Platforms.* Mol Biol Evol, 2018. **35**(6): p. 1547-1549.
105. Muckelbauer, J.K., et al., *Structure determination of coxsackievirus B3 to 3.5 A resolution.* Acta Crystallogr D Biol Crystallogr, 1995. **51**(Pt 6): p. 871-87.
106. Wessely, R., et al., *Cardioselective infection with coxsackievirus B3 requires intact type I interferon signaling: implications for mortality and early viral replication.* Circulation, 2001. **103**(5): p. 756-61.
107. Cameron-Wilson, C.L., et al., *Nucleotide sequence of an attenuated mutant of coxsackievirus B3 compared with the cardiovirulent wildtype: assessment of candidate mutations by analysis of a revertant to cardiovirulence.* Clin Diagn Virol, 1998. **9**(2-3): p. 99-105.
108. Gauntt, C.J., et al., *Temperature-sensitive mutant of coxsackievirus B3 establishes resistance in neonatal mice that protects them during adolescence against coxsackievirus B3-induced myocarditis.* Infect Immun, 1983. **39**(2): p. 851-64.
109. Domingo, E., et al., *Nucleotide sequence heterogeneity of an RNA phage population.* Cell, 1978. **13**(4): p. 735-44.
110. Burch, C.L. and L. Chao, *Evolvability of an RNA virus is determined by its mutational neighbourhood.* Nature, 2000. **406**(6796): p. 625-8.
111. Borderia, A.V., et al., *Group Selection and Contribution of Minority Variants during Virus Adaptation Determines Virus Fitness and Phenotype.* PLoS Pathog, 2015. **11**(5): p. e1004838.
112. Reisdorph, N., et al., *Human rhinovirus capsid dynamics is controlled by canyon flexibility.* Virology, 2003. **314**(1): p. 34-44.
113. Groarke, J.M. and D.C. Pevear, *Attenuated virulence of pleconaril-resistant coxsackievirus B3 variants.* J Infect Dis, 1999. **179**(6): p. 1538-41.
114. Pevear, D.C., et al., *Activity of pleconaril against enteroviruses.* Antimicrob Agents Chemother, 1999. **43**(9): p. 2109-15.
115. Pan, J., et al., *Specificity of coxsackievirus B3 interaction with human, but not murine, decay-accelerating factor: replacement of a single residue within short consensus repeat 2 prevents virus attachment.* J Virol, 2015. **89**(2): p. 1324-8.
116. Gnadig, N.F., et al., *Coxsackievirus B3 mutator strains are attenuated in vivo.* Proc Natl Acad Sci U S A, 2012. **109**(34): p. E2294-303.
117. Olofsson, S. and T. Bergstrom, *Glycoconjugate glycans as viral receptors.* Ann Med, 2005. **37**(3): p. 154-72.

CURRICULUM VITAE

April L Barnard

Summary of qualifications

- Experienced research scientist in microbiology and immunology, with a focus in virology.
- Additional research in integrated and cellular physiology as well as surgery.
- Well-versed in molecular in vitro techniques such as PCR, ELISA, and other serological tests as well as whole-animal models in virology and physiology.
- Knowledgeable regarding enteric viruses and pathogenic enteric bacteria.
- Excellent verbal and written skills, strong interpersonal skills with ample leadership experience.

Experience

Indiana University, Indianapolis, IN **Sept 2017-Aug 2020**

Robinson Lab explores intestinal enteric virus replication with an emphasis in virus/gut microbiota interactions.

Graduate student, Department of Microbiology and Immunology

- Research focused on delineating mechanisms that underlie the sex bias seen in CVB3 infection.
- Demonstrated sex bias in CVB3 intestinal replication using novel mouse model.
- Adapted novel oral inoculation model to demonstrate that sex and site of replication should be considered in investigations of enteric viral replication and pathogenesis.

- Used molecular biology, cell biology, mouse models, histology, flow cytometry and novel imaging techniques extensively.
- Designed and created viral mutants and viral luciferase assays.
- Participated in preparing and writing of operating grant applications (NIH and AAAS)
- Trained graduate students, medical fellow, and technicians in qPCR, cytokine arrays, and mutagenesis.
- Trained and supervised technicians and students in proper mouse gavage techniques.

Indiana University, Indianapolis, IN **May 2016-June 2017**

Tune Lab focused on the molecular mechanisms underlying the association of obesity, coronary flow, and cardiovascular dysfunction.

Graduate student, Department of Cellular and Integrative Physiology

- Investigated the effects of Leptin, GLP, and RANKL in coronary artery calcification.
- Performed both survival and terminal coronary artery bypass procedures on Ossabaw swine as well as domestic porcine model.
- Pharmacologically investigated the effects of RANKL and OPG on coronary arteries using tissue bath/perfusion system.

Ivy Tech Community College, Indianapolis, IN **Aug 2016-Sept 2020**

Facilitated instruction for Microbiology BIOL 201 courses.

Adjunct Instructor, Biotechnology Department

- Teach both the lab and lecture portions of BIOL 201, a notoriously challenging nursing program pre-requisite course.
- Designs and implements lectures encompassing microbiology concepts ranging from DNA replication to monoclonal antibody production.
- Facilitates hands-on guidance with scientific experiments including PCR, ELISA, and bacterial transformations.

Education

Indiana University McKinney School of Law, Indianapolis, IN **2020-**

JD Law Professional

- Intellectual Property Law

Indiana University earned at

Indiana University-Purdue University Indianapolis **2020**

MS in Microbiology and Immunology

- Genetic Determinants of Coxsackievirus B3 Pathogenesis

Indiana University, New Albany, IN **2015**

BS, Department of Biology, cum laude

AA, Department of Chemistry, cum laude

Skills & Techniques

- **Molecular biology:** recombinant DNA techniques, western blotting, RT-qPCR, viral transduction, liposome mediated transfection, electroporation
- **Surgical:** independently perform survival as well as terminal coronary bypass procedures in swine, mouse ovariectomy and castrations, and perfusions. Perform or assist in multi-organ harvest in human, swine, and mouse. Extremely proficient in coronary artery dissection from Ossabaw and domestic swine heart
- **Cellular biology:** Isolation and culture of cardiomyocytes and intestinal cell lines, *in situ* hybridization (RNA scope), nano luciferase bioluminescence, flow cytometry, DNA, RNA, protein extraction and purification
- **Microscopy:** light microscopy, fluorescent/laser confocal microscopy
- **Virology:** Amplification and purification of picornavirus and lentivirus for *in vivo* and *in vitro* work, plaque assay, one-step growth curves, and mutagenesis.
- **Coronary artery biology:** Lentivirus injection, whole animal perfusion, length-tension isometric ring bath.
- **Histology:** Immunocytochemistry, H&E staining, Von Kossa, Wright-Geimsa, Ki-67, cryosection.
- **Computer skills:** Microsoft Office, Photoshop, Prism, statistical analysis and modeling using R studio, Python.

Memberships

- American Association for the Advancement of Science 2019
- American Society for Virology 2018
- Indiana Physiological Society 2016

- American Physiological Society 2016
- Indiana Academy of Sciences 2014

Leadership

President *Biomedical Graduate Student Advocacy Association* 2019

President *Department of Microbiology and Immunology Grad Rep* 2018

President *IUSM Chapter 314 Action* 2017

Presentations

- **American Society for Virology** (speaker) 2019

  The role of sex hormones on intestinal Coxsackievirus B3 replication

- **Midwest Microbial Pathogen Conference** (poster) 2018

  The role of biological sex in Coxsackievirus B3 infection and pathogenesis

- **Experimental Biology** (poster) 2017

  Role of Receptor Activator of Nuclear Factor kB Ligand (RANKL) in Coronary Smooth Muscle Contraction and Medial Calcification

- **Indiana Physiological Society Conference** (poster) 2016

  SERCA inhibition attenuates medial thickening in an organ culture model of coronary artery disease

- **Indiana Academy of Sciences Conference** (poster) 2015

  Decellularization and re-endothelialization of mouse hearts using induced pluripotent stem-cell derived cardiovascular progenitor cells

Publications

- Alexander M. Kiel, Adam G. Goodwill, Jillian N. Noblet, **April L. Barnard**, Daniel J. Sassoon, Johnathan D. Tune. Regulation of myocardial oxygen delivery in response to graded reductions in hematocrit: role of K+ channels. *Basic Res Cardiol* (2017) 112:65
- Leni Moldovan, **April Barnard**, Chang-Hyun Gil, Y. Lin, Maria B. Grant, Mervin C. Yoder, Nutan Prasain, Nicanor I. Moldovan. iPSC-Derived Vascular Cell Spheroids as Building Blocks for Scaffold-Free Biofabrication. *Biotechnology Journal*. (2017): DOI: 10.1002/biot.201700444
- Huang J, Donneyong M, Trivedi J, **Barnard AL**, Chaney J, Dotson A, Raymer S, Cheng A, Hong, Liu and Slaughter MS. Preoperative Aspirin Use and its Effect on Adverse Events in Patients Undergoing Cardiac Surgery. *Annals of Thoracic Surgery*. 99(6), 2015